INVESTIGATION OF LINEAR PHASED ARRAYS FOR HYPERTHERMIA APPLICATIONS

BY

PAUL JOSEPH BENKESER

B.S., Purdue University, 1981

THESIS

Submitted in partial fulfillment of the requirements
for the degree of Master of Science in Electrical Engineering
in the Graduate College of the
University of Illinois at Urbana-Champaign, 1983

Urbana, Illinois

TABLE OF CONTENTS

ACKNOWLEDGEMENTS

The author would like to express gratitude to his advisors Dr. Charles Cain and Dr. Leon Frizzell for their encouragement and guidance throughout the course of the work for this thesis. Special thanks are due to Mr. Steven Foster for his invaluable assistance in the design of the hardware, to Dr. Bruce Wheeler for help in fabricating the array, and to Mr. Bill McNeill for his help in building the array housing. Thanks also to Mr. Michael Haney and Dr. Ronald Johnston for their assistance in solving software problems, to Mr. Joseph Cobb for his assistance in construction of the hardware, and to Mr. Robert Cicone and Mr. Michael Borrelli for their help with the drawings and photographs appearing in this thesis. Sincere thanks is extended to Mrs. Wanda Elliott, whose assistance in preparation and typing of this thesis was greatly appreciated. The author would also like to thank his parents for all the love, encouragement, and support that they have given him throughout his educational career.

CHAPTER I

INTRODUCTION

In the past few years there has been increasing interest shown in hyperthermia research for cancer therapy. It has been found that the use of heat alone, or in conjunction with chemotherapy or radiation, may produce some therapeutic gain (Hynynen et al., 1981). Many different techniques, such as microwaves, ultrasound, radiofrequency currents, water bath immersion, and perfusion with heated blood, have been used to produce hyperthermia. The production of hyperthermia requires well controlled heating capabilities, particularly for generating local hyperthermia, and an accurate temperature monitoring system. Each of the techniques listed above have different physical constraints that can limit their applicability to the production of local hyperthermia to particular tumor types and locations. No one modality is applicable to all tumor locations.

Since ultrasound can be easily focused, it is currently the best modality for creating a controllable and uniform temperature rise to a preselected volume of target tissue or tumor (Lele, 1975). The absorption of ultrasound is such that the ultrasonic frequency range useful to hyperthermia is approximately 500 kHz to 1 MHz or higher depending on tumor depth. Since for this frequency range the focal spot size can be considerably smaller than the region to be heated, a tightly focused beam can be swept with a continuously changing position as a function of time producing the desired heating patterns (Christensen and Durney, 1981). The beam has been swept by mechanically moving the

applicator (Lele, 1975). An alternate way to control the movement of the beam would be to use an array of ultrasonic radiating elements. The focus of a beam produced by an array can be controlled by varying electronically the phases of the signals driving the elements. By changing the phases of each of the elements, the focus of the beam can be moved to follow any desired pattern. This allows movement of the focus in three dimensions. One possible approach would be to use a microcomputer system to control the phased array. If data from a temperature measurement system were fed into the microcomputer, a closed loop system could be realized. The temperature measurements would indicate where the hot and cold spots lie in the site being heated. The microcomputer would then adjust the swept pattern of the ultrasonic beam to maintain the desired temperature gradient across the site. This phased array system would be much less mechanically complex than the mechanically swept system.

The work for this thesis was directed toward developing a linear ultrasonic array using a digital phase shifting network to control the phase of the signal that drives each element of the array. Ultimately a series of multiplexed linear arrays could be used to cover a 15 cm square treatment field with a focused beam. This series of linear arrays would have to provide about 300 W of tissue heating power in order to cause a therapeutically significant temperature rise in the treatment field in a reasonable length of time.

The intensity of the focused beam in the initial design was only sufficient to measure the resulting ultrasonic field pattern. The digital phase shifting network was controlled by a

Perkin-Elmer 7/32 minicomputer. Theoretical field patterns were computed and compared to the actual field patterns obtained using a hydrophone probe and amplifier system.

CHAPTER II

TRANSDUCER DESIGN

2.1. Theory of Operation of a Linear Array

2.1.1. Beam Forming

The linear array was the first multielement system to appear commercially. The linear array consists of a piezoelectric ceramic divided into closely spaced rectangular strips arranged side by side. These were originally designed for use in real time medical imaging. The theory for linear arrays used in imaging can be applied to hyperthermia applications since the only difference is in the intensity levels of the focused beam.

The radiation pattern of an individual array element is an important criterion in the design of transducer array elements. The rectangular element produces a beam that is slightly different than the beam produced by a circular element. The individual element radiation pattern is described by Selfridge et al. (1980)

$$E(\theta) = [\mathrm{sinc}(\frac{\pi w}{\lambda} \sin\theta)][\cos\theta] \qquad (2.1)$$

where θ is the angle with respect to the normal to the element and λ is the wavelength of the acoustic wave in the propagating medium. Figure 2.1 illustrates the parameters used in defining a phased array. Equation 2.1 indicates that, however narrow the width of the element, the response will be zero at $\theta = \pi/2$. As the element narrows, the angular response broadens. Moreover, if the value of λ is decreased (due to an increase in frequency), the beam will become narrower. Therefore, increasing both element

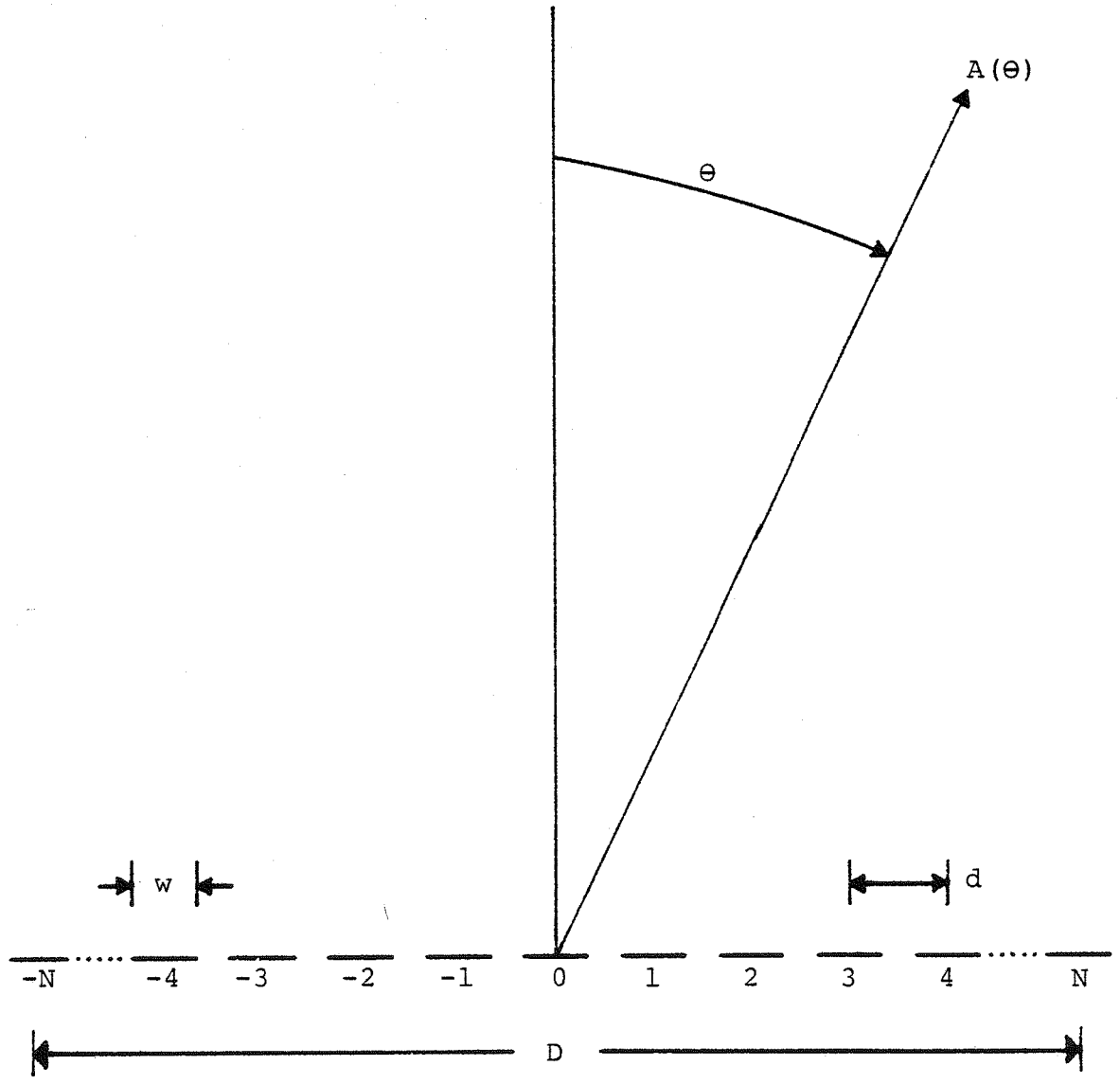

Figure 2.1. Definition of Linear Phased Array Parameters (Larson, 1981)

width and frequency will result in a more directional radiation pattern from an individual element.

Focusing is achieved by controlling the phase of the electrical signal applied to each element of the array. The phases are adjusted so that the acoustical signals from each element reach a common point (focal point) at the same time. A linear array can move the focal point in the x and z directions (see Fig. 2.2).

The length of the near field of the array, NF, is approximately

$$NF = \frac{D^2}{4\lambda} \qquad (2.2)$$

where D is the total width of the array (Aero-Tech, 1981). The near field of the array is the nondiverging portion, under conditions of a common phase to each element, of the radiated field. The far field divergence angle, Φ, under the same conditions, is given by

$$\Phi = \arcsin(\frac{\lambda}{D}) \quad . \qquad (2.3)$$

Therefore, an increase in the total width of the array will result in an increased length of the near field and a reduced angle of divergence. This effectively yields a narrower radiation pattern (Aero-Tech, 1981). Frequency also affects the array beamwidth. An increase in frequency (decrease in λ) will cause a lengthening of the near field and a decrease in the divergence angle. This again results in a narrower array radiation pattern.

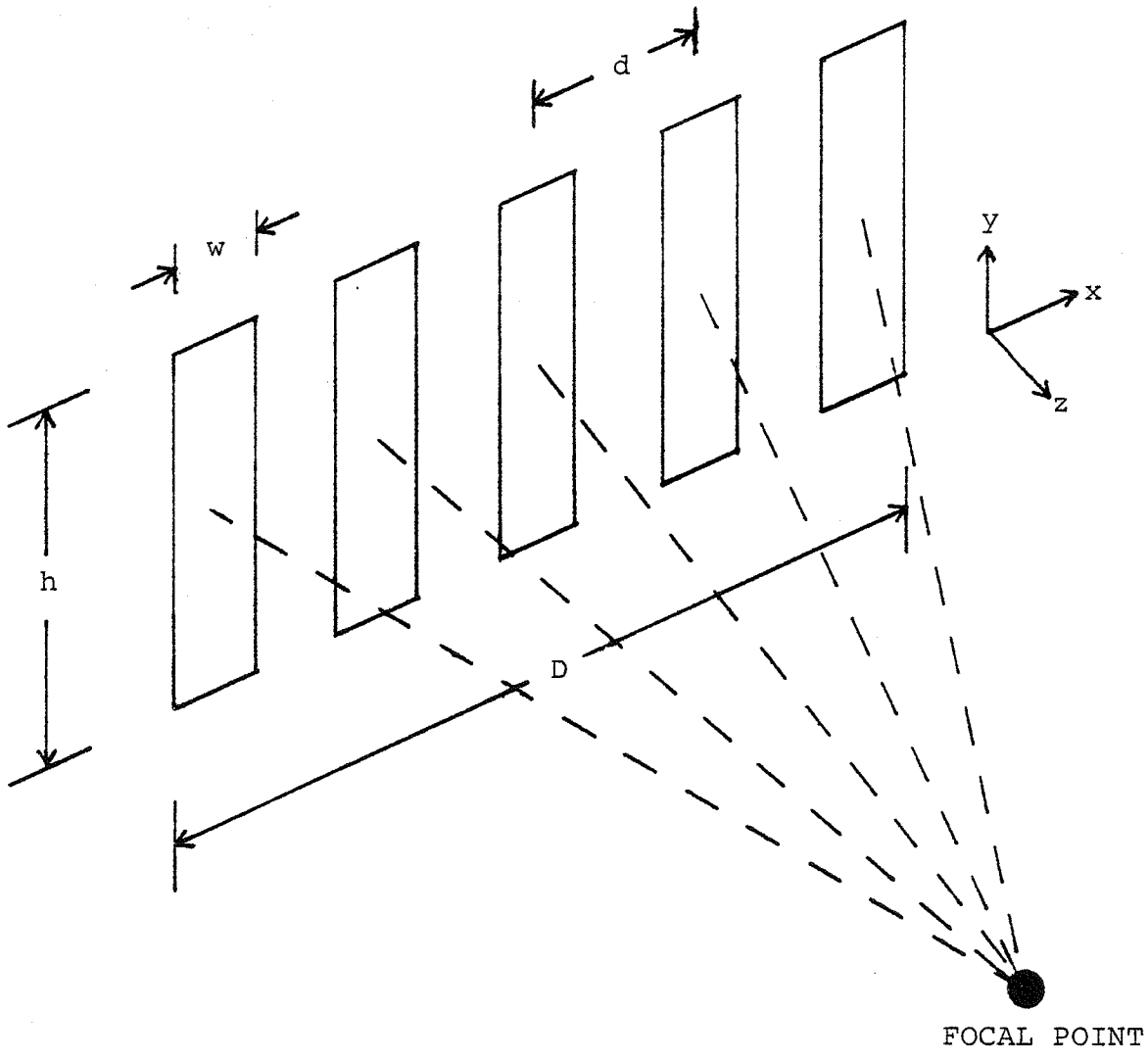

Figure 2.2. Definition of Linear Phased Array Parameters

2.1.2. Secondary Lobes

Secondary lobes are the most serious problem in linear arrays. There are two types of secondary lobes: side lobes and grating lobes. Both are areas of ultrasonic energy occurring outside of the focused main beam. In hyperthermia applications significant secondary lobes can cause heating in areas where it was not intended. Side lobes are a function of frequency and active area considerations. Generally, more and smaller elements will result in lower amplitudes of the side lobes (Aero-Tech, 1981). These side lobes are not of much concern in hyperthermia applications since the amplitudes of these lobes are generally 60 dB down from that of the main beam.

Grating lobes are a much more significant problem. These lobes are a result of the regular, periodic spacing of the elements of the array. The following equation gives the location of the grating lobes with reference to the main beam

$$\psi = \arcsin\left(\frac{m\lambda}{d}\right) \qquad (2.4)$$

where ψ is the angle in degrees from the main beam's central axis, m is the order of the grating lobe, and d is the on center spacing of the array elements. To minimize the effects of the grating lobes it is necessary to make the angle ψ approach 90^{o} from the main beam axis. This can be accomplished by making d less than λ ($\psi > 90^{o}$). The farther off the main beam's axis the grating lobes are, the more their amplitudes are reduced relative to that of the main beam (Aero-Tech, 1981).

2.1.3 Beam Steering

There is a direct correlation between the radiation pattern of a single element and the radiation pattern of the total array. The radiation pattern of the array is the product of the single element radiation pattern (Eq. 2.1), and the array radiation pattern A(θ) where

$$A(\theta) = \frac{\sin \frac{\pi(2N+1)d}{\lambda}(\sin\theta - \sin\theta_o)}{\sin \frac{\pi d}{\lambda}(\sin\theta - \sin\theta_o)} \tag{2.5}$$

where 2N + 1 is the total number of elements, θ_o is the beam steering angle, and θ is the observation angle. The far field pattern for the array will then be

$$P(\theta) = A(\theta) \times E(\theta) \tag{2.6}$$

which in terms of array parameters is

$$P(\theta) = \frac{\sin \frac{\pi(2N+1)d}{\lambda}(\sin\theta - \sin\theta_o)}{\sin \frac{\pi d}{\lambda}(\sin\theta - \sin\theta_o)} \operatorname{sinc}\left(\frac{\pi w}{\lambda}\sin\theta\right) \cos\theta \tag{2.7}$$

Equation 2.7 gives the far field pattern in the x - z plane (Fig. 2.2). In the y - z plane the far field pattern is the sinc pattern

$$P(y_z) = \operatorname{sinc}\left(\frac{y_z h}{\lambda_z}\right) \tag{2.8}$$

resulting from an array of height h (Macovski, 1979).

2.2. Plotting the Theoretical Far Field Pattern

The theoretical far field pattern program (listed in Appendix A) plots the far field pattern for a linear phased array. The dimensions of the array (element size, spacing and number) and the desired focal point are the inputs. The outputs are the phase shifts needed for each element to achieve the desired focal point, and a two dimensional plot of the far field pattern in either the x - z or y - z plane. The amplitude of the intensity in the plotted response is given in decibels relative to that of the main beam. A program to plot the near field pattern for a linear phased array has not yet been developed.

2.3. Array Parameters

There are several array parameters that control the far field patterns of the array. These are frequency, width and height of an element, on-center spacing between elements, and depth of focus. These parameters are all interdependent and proper choices are needed to achieve a desired far field pattern.

2.3.1. Frequency

For this design the range of frequencies is limited to 500 kHz to 1 MHz. The digital phase shifting network, as discussed in Chapter 3, limits the maximum frequency to about 1 MHz. Frequencies below 500 kHz will not yield any increase in power deposition per unit volume (Christensen and Durney, 1981). The focal spot size at frequencies less than 500 kHz becomes unacceptably large. For these reasons, the lower frequency limit was chosen to be 500 kHz. Generally, as the frequency is

increased, more and narrower elements are required to minimize problems with grating lobes.

2.3.2. Width and Height of Element

The elements should be designed as large as possible because larger elements can handle more power before failing. The maximum width of an element is limited by the depth of focus and the maximum element on-center spacing. The height of an element is determined by the number of linear arrays in the applicator, and the desired treatment field size. The beamwidth of the focal spot in the unfocused dimension is controlled by the height of the elements. It is desired to have the -3dB points of focal spot in the unfocused dimension of each linear array overlap. This will ensure that the total area of the treatment field can be covered by the focused beam. The -3dB beamwidth in the unfocused dimension must be greater than the height of the elements to ensure total coverage of the treatment field. This -3dB beamwidth dictates how many linear arrays will be needed in order to cover the desired treatment field. For instance, if the -3dB beamwidth was 30 mm and the desired treatment field was 150 mm in the unfocused dimension, five linear arrays would be needed to cover the field.

2.3.3. Element Spacing

The on-center spacing between elements should be kept to a minimum. The greater the spacing, the greater the problem with grating lobes. Increasing the frequency will require decreasing the on-center spacing in order to minimize problems with grating

lobes. The decrease in the on-center spacing results in narrower elements which cannot handle as much power.

2.3.4. Depth of Focus

The depth of the focal point can be varied to help reduce the problem of grating lobes. Increasing the depth of focus increases the angle of the grating lobes from the main beam. If the grating lobes are reduced more than 3dB in intensity than the main beam, their contribution to undesired heating should be acceptable. Grating lobes that are reduced less than 3dB from the main beam, but outside the treatment field, can be eliminated through the use of an appropriate mask made of an ultrasonic absorbing material. The intensity of the grating lobes relative to the main beam does not decrease with increasing depth of focus. The depth of focus can be increased by using a degassed water interface ("bolus") between the applicator and the patient. However, there can be problems with using a large degassed water interface. First, it can make the applicator setup bulky and difficult to handle. Secondly, and more importantly, nonlinearities can develop in the focused beam due to the length of the path traveled through the degassed water. These nonlinearities could cause a defocusing effect on the main beam. The minimum depth of focus is determined by the length of the near field as was discussed in Sec. 2.1.1.

2.4. Determining Optimal Array Designs

Several designs for the linear arrays were examined using the theoretical far field pattern program. These designs were based on maximizing the power handling capabilities of the array. The largest possible element size consistent with low level grating

lobes was used in each case. The maximum number of elements in the array was arbitrarily chosen to be fifteen. The maximum allowable beamwidth in the focused direction was 2.5 cm. The size of the treatment field was 15 cm x 15 cm. Arrays were designed to be used with and without masks. Design frequencies of 500 kHz and 1 MHz were chosen to cover the range of possible frequencies. In Figs. 2.3 through 2.14 three far field patterns are plotted for each design. The first plot shows the far field pattern in the x - z plane (focused) for zero degrees beam steering. The second plot is the pattern in the y - z plane (unfocused) also with zero degrees beam steering. The third plot is in the x - z plane with the appropriate beam steering angle to move the main beam to the edge of the treatment field. The shape of the far field pattern in the y - z plane is not affected by the change in the beam steering angle.

2.4.1. 500 kHz Designs

Figures 2.3 through 2.5 show the far field patterns and array parameters for a design that would require a mask. The far field patterns and array parameters for the design using no mask are found in Figs. 2.6 through 2.8. The use of the mask allows for wider and fewer elements but the resulting beamwidth is approximately 2.5 cm while the beamwidth for the design without a mask is about 1.9 cm. The height of the element is the same for both designs. The beamwidth in the unfocused dimension (Figs. 2.4 and 2.7) is approximately 5.0 cm. This means that three linear arrays would have to be used to cover the treatment field. For simultaneous activation of each array, the design using a mask

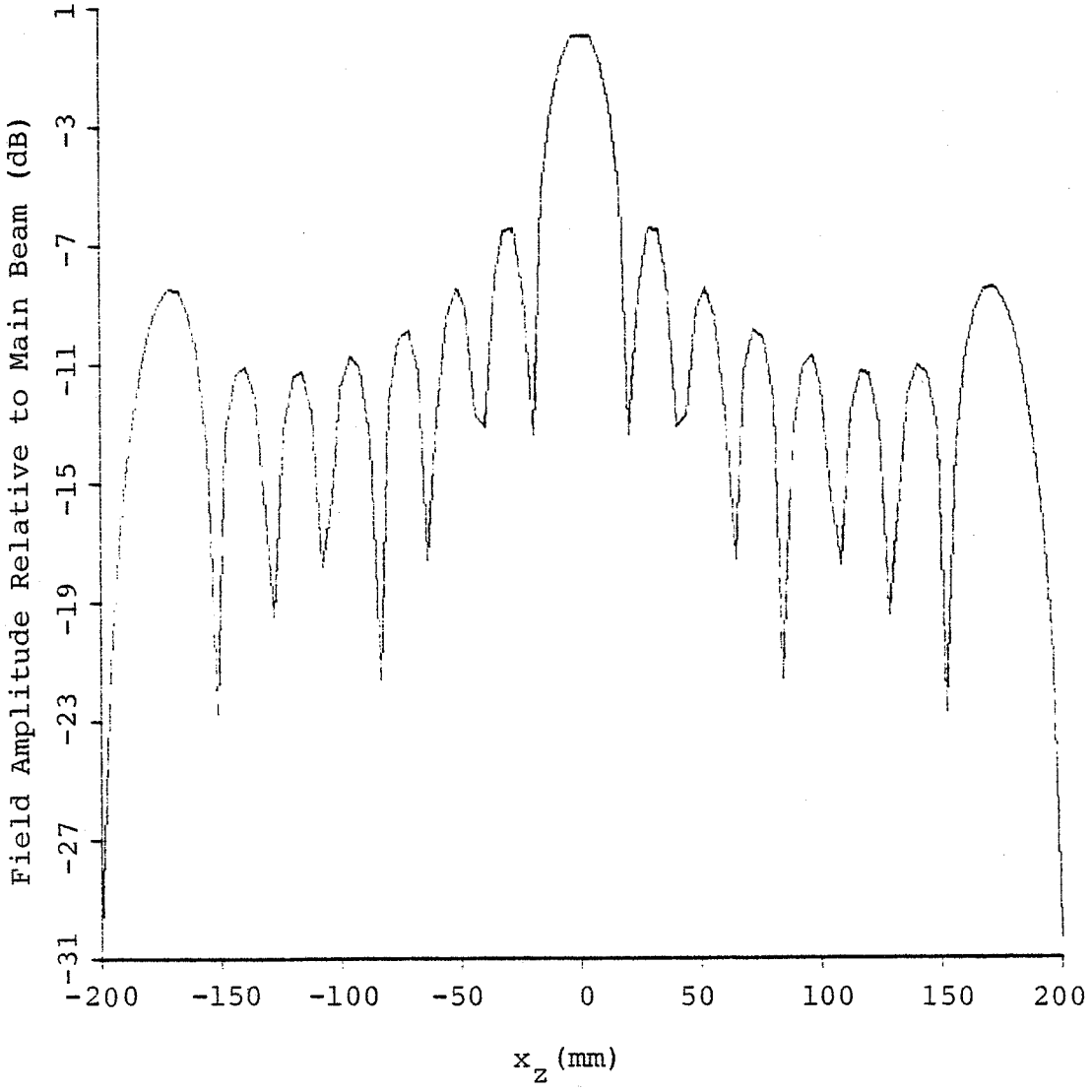

Figure 2.3. Theoretical Far Field Pattern Requiring a Mask

Number of Elements = 8

Element Width = 8.0 mm

Element Height = 36.0 mm

Element Spacing = 9.0 mm

Depth of Focus = 500.0 mm

Beam Steering = 0.0 °

Frequency = 500.0 kHz

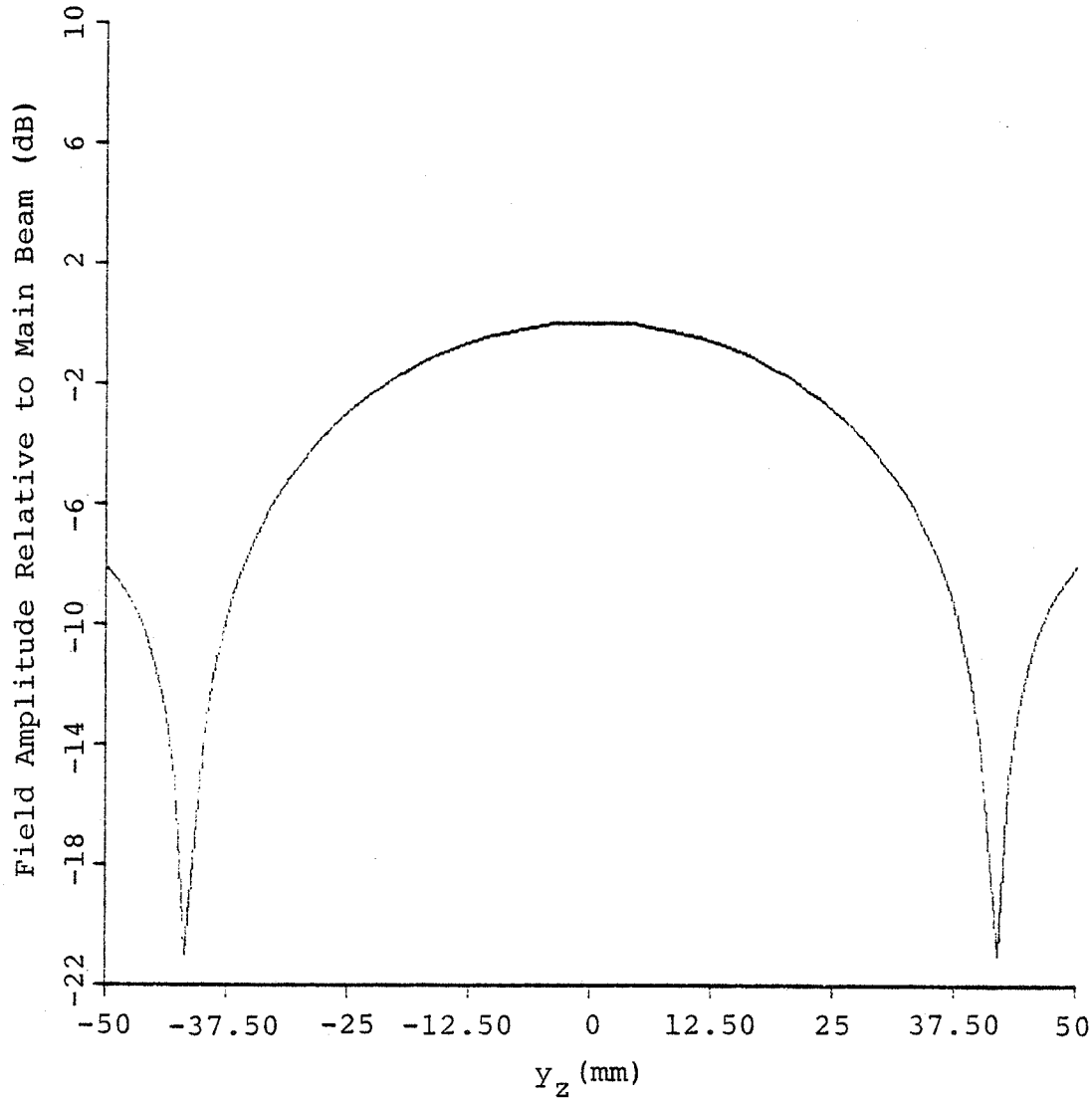

Figure 2.4. Theoretical Far Field Pattern Requiring a Mask

Number of Elements = 8

Element Width = 8.0 mm

Element Height = 36.0 mm

Element Spacing = 9.0 mm

Depth of Focus = 500.0 mm

Beam Steering = 0.0°

Frequency = 500.0 kHz

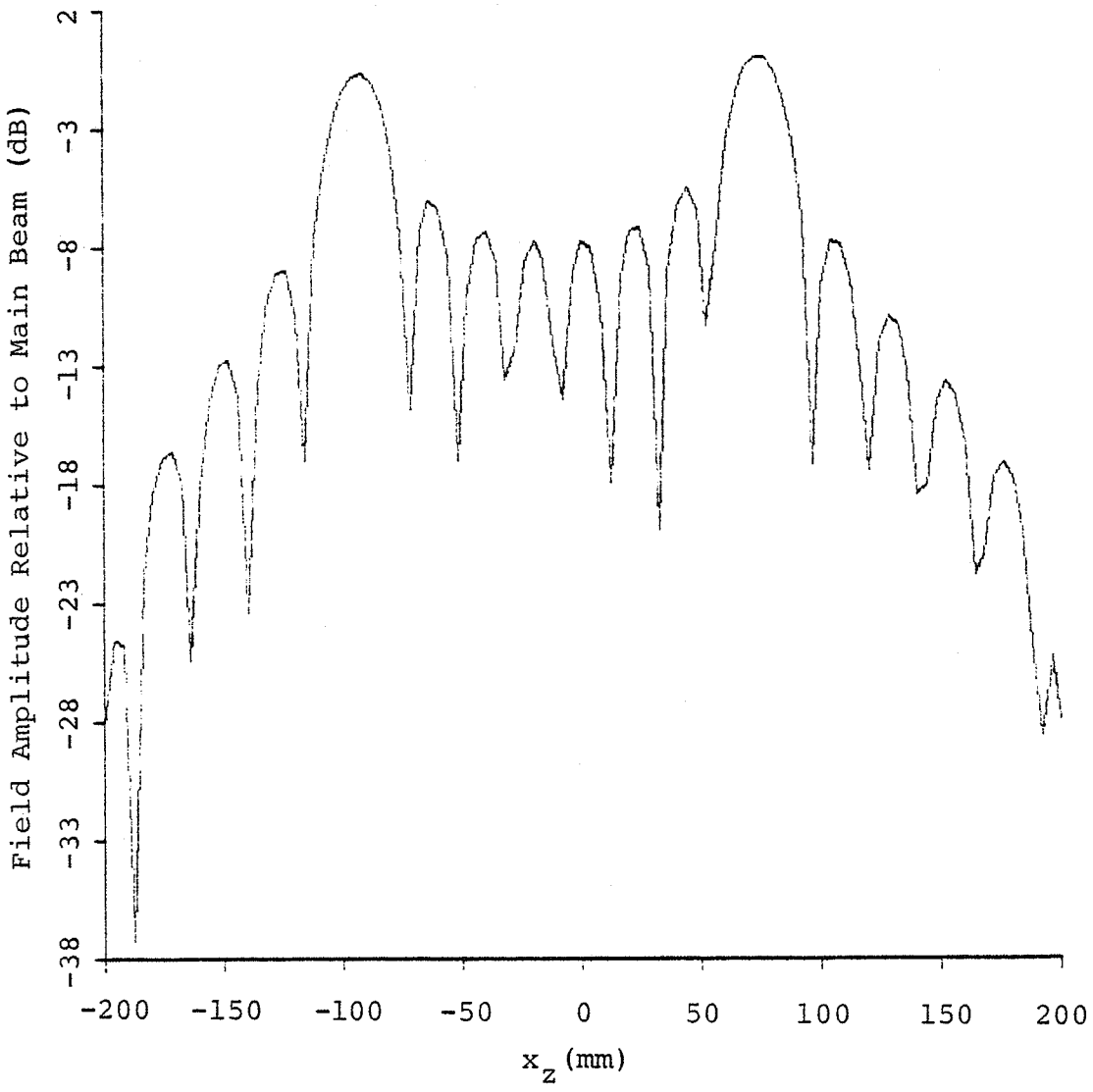

Figure 2.5. Theoretical Far Field Pattern (with Beam Steering) Requiring a Mask

Number of Elements = 8

Element Width = 8.0 mm

Element Height = 36.0 mm

Element Spacing = 9.0 mm

Depth of Focus = 500.0 mm

Beam Steering = 8.5°

Frequency = 500.0 kHz

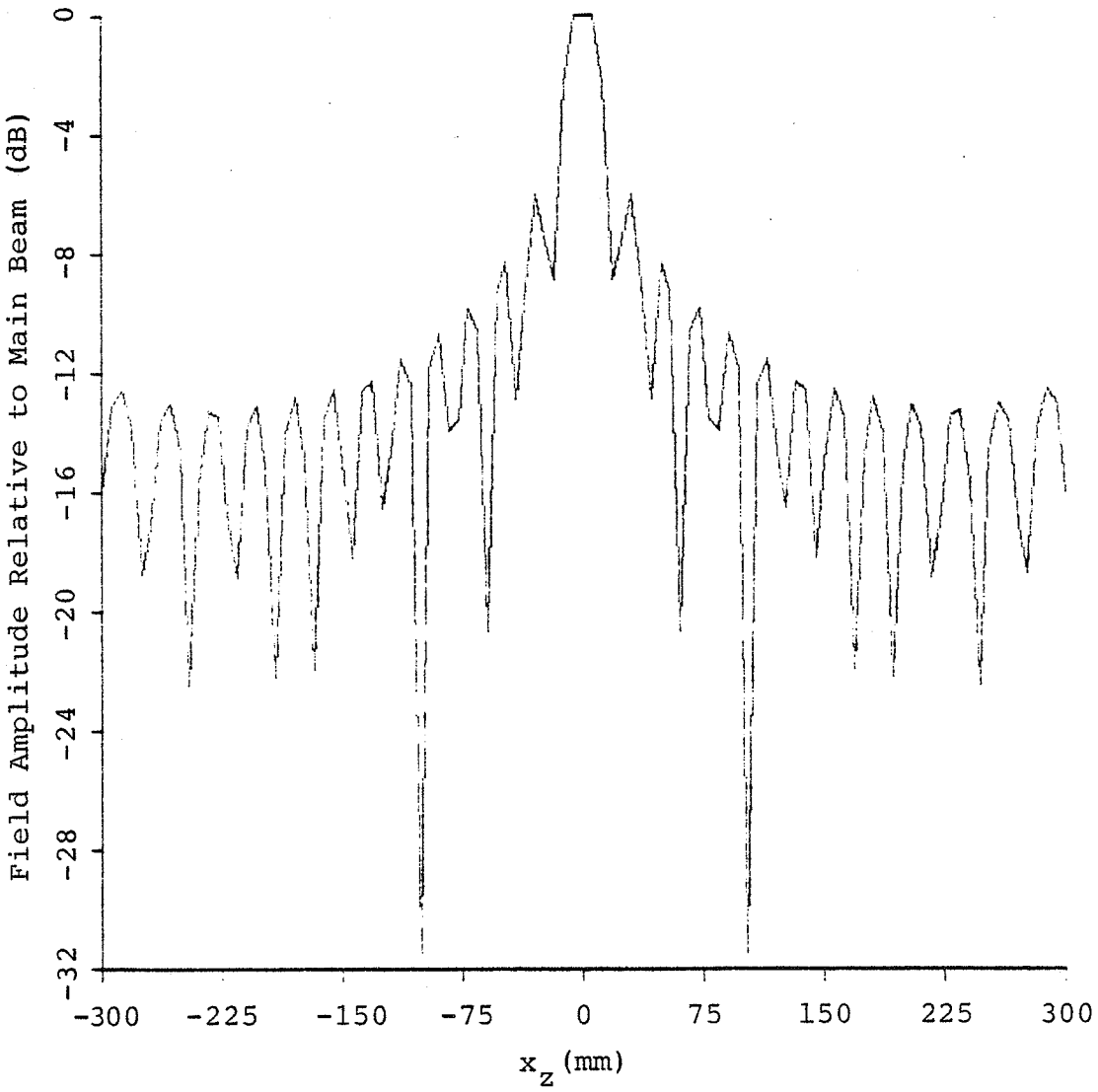

Figure 2.6. Theoretical Far Field Pattern

Number of Elements = 15

Element Width = 4.0 mm

Element Height = 36.0 mm

Element Spacing = 5.0 mm

Depth of Focus = 500.0 mm

Beam Steering = 0.0°

Frequency = 500.0 kHz

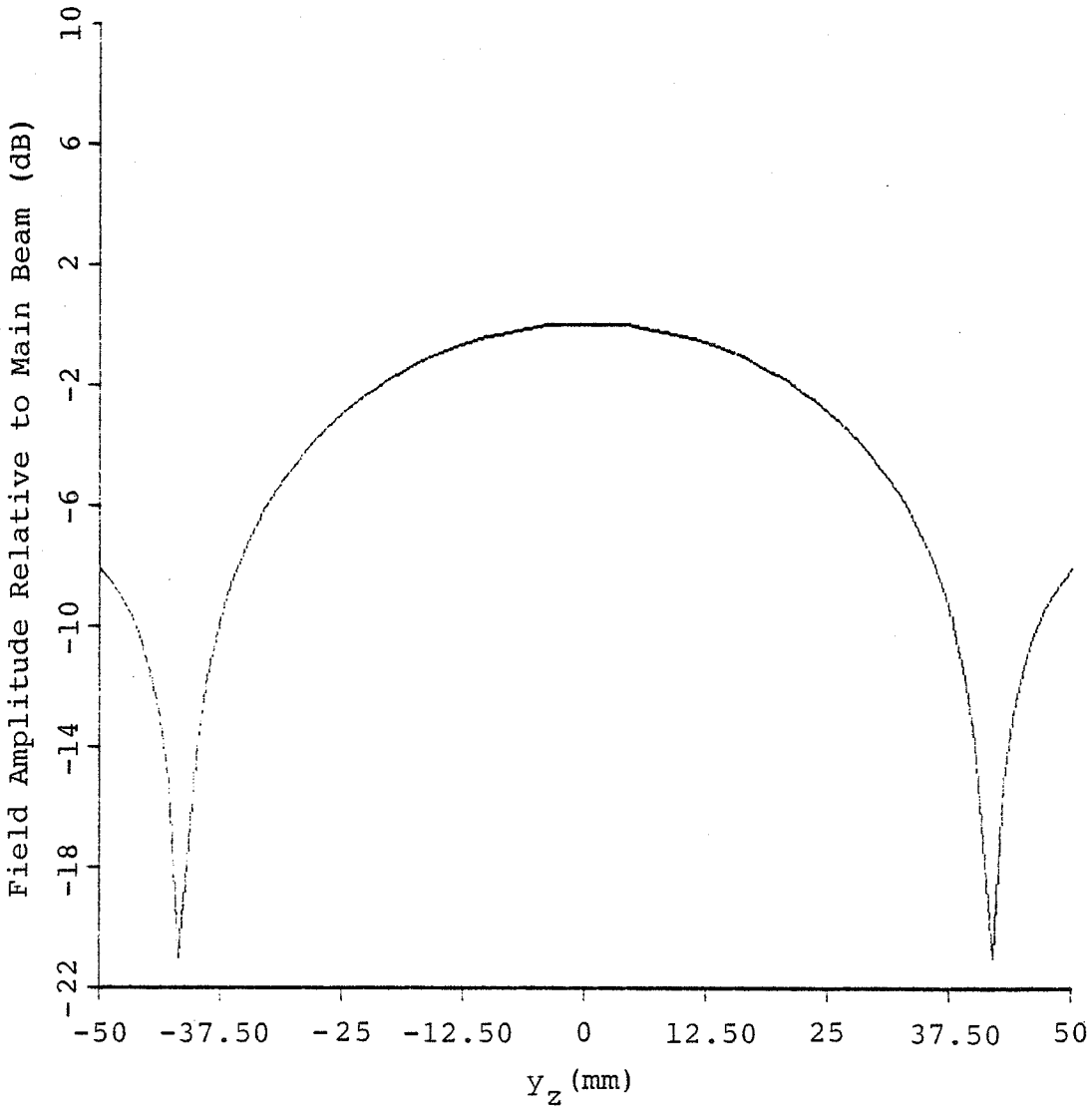

Figure 2.7. Theoretical Far Field Pattern

Number of Elements = 15

Element Width = 4.0 mm

Element Height = 36.0 mm

Element Spacing = 5.0 mm

Depth of Focus = 500.0 mm

Beam Steering = 0.0°

Frequency = 500.0 kHz

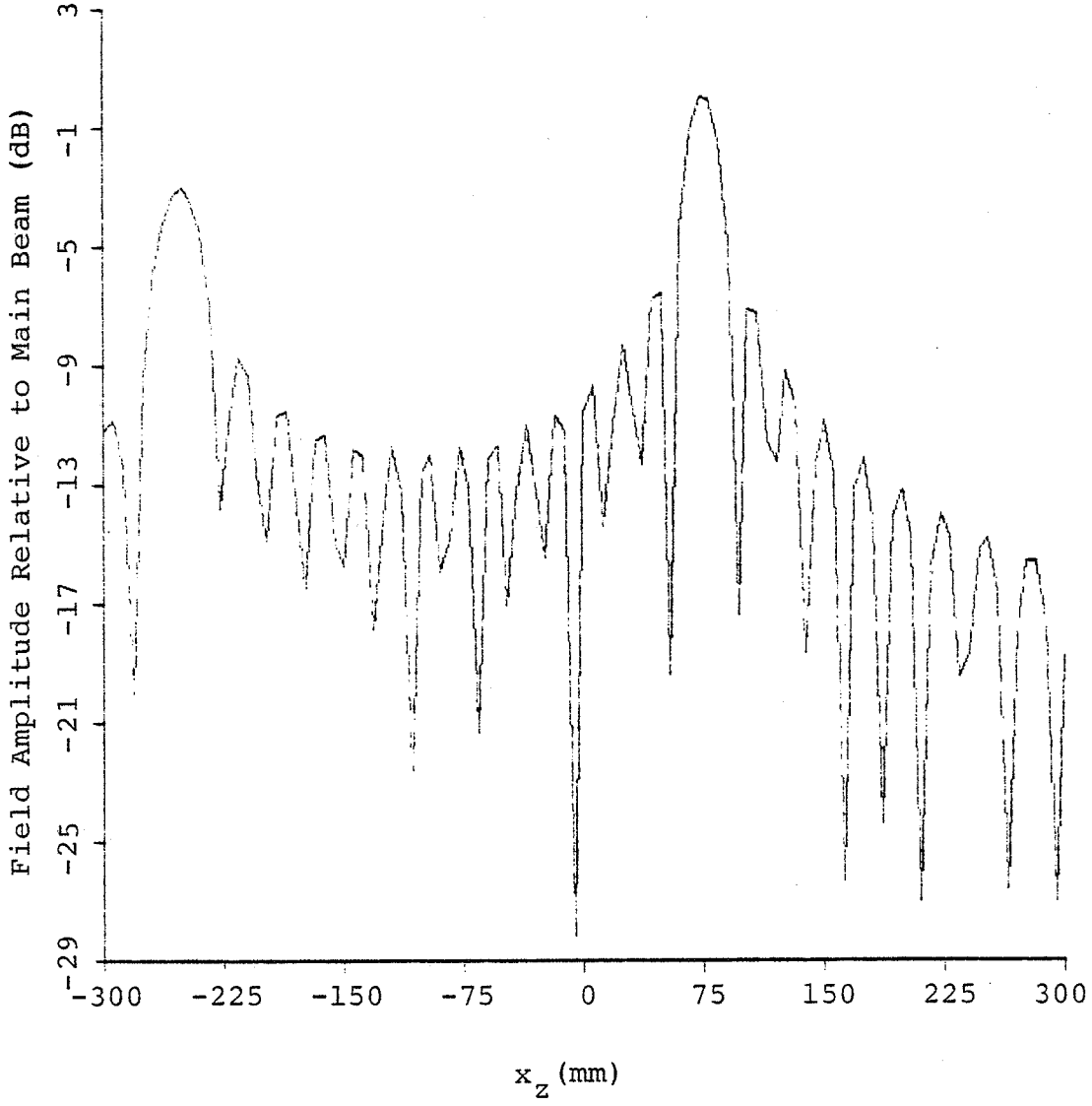

Figure 2.8. Theoretical Far Field Pattern (with Beam Steering)

Number of Elements = 15

Element Width = 4.0 mm

Element Height = 36.0 mm

Element Spacing = 5.0 mm

Depth of Focus = 500.0 mm

Beam Steering = 8.5^{o}

Frequency = 500.0 kHz

therefore would require 24 amplifiers to drive all of the elements, while the design using no mask would require 45 amplifiers.

2.4.2. 1 MHz Designs

Figures 2.9 through 2.11 list the array parameters and show the far field patterns for a design that would require a mask. The array parameters and far field patterns for a design using no mask are found in Figs. 2.12 through 2.14. As was the case with the 500 kHz designs, the use of a mask allows for wider and fewer elements. The beamwidth of the design using a mask is approximately 1.7 cm, while the beamwidth for the design without a mask is about 2.5 cm. The beamwidth in the unfocused dimension (Figs. 2.10 and 2.13) is approximately 3.08 cm. Since the depth of focus is not as large, these beamwidths are in general not any larger than those in the 500 kHz designs. This requires that five linear arrays be used to cover the whole treatment field. For simultaneous activation of each array, the design using a mask would then require 55 amplifiers while the design using no mask would require 75 amplifiers.

2.4.3. Optimal Design

Of the designs discussed in Sec. 2.4.1 and 2.4.2, the optimal design in terms of least number of amplifiers and largest element size is the 500 kHz design using a mask. This is considered the optimal design since these are the largest elements possible and this array will be able to handle more power than any of the others.

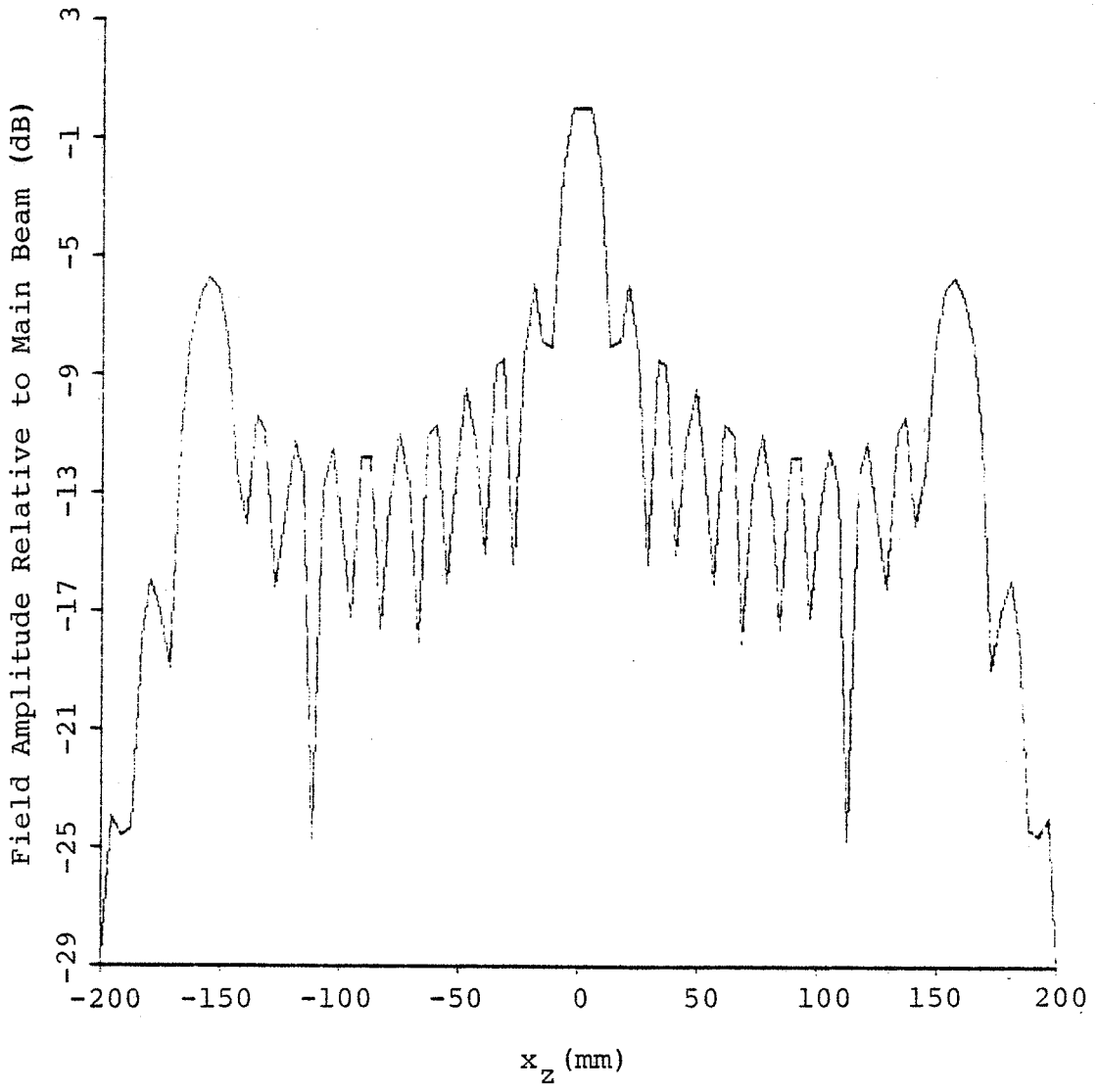

Figure 2.9. Theoretical Far Field Pattern Requiring a Mask

Number of Elements = 11

Element Width = 4.0 mm

Element Height = 30.0 mm

Element Spacing = 5.0 mm

Depth of Focus = 500.0 mm

Beam Sterring = 0.0°

Frequency = 1.0 MHz

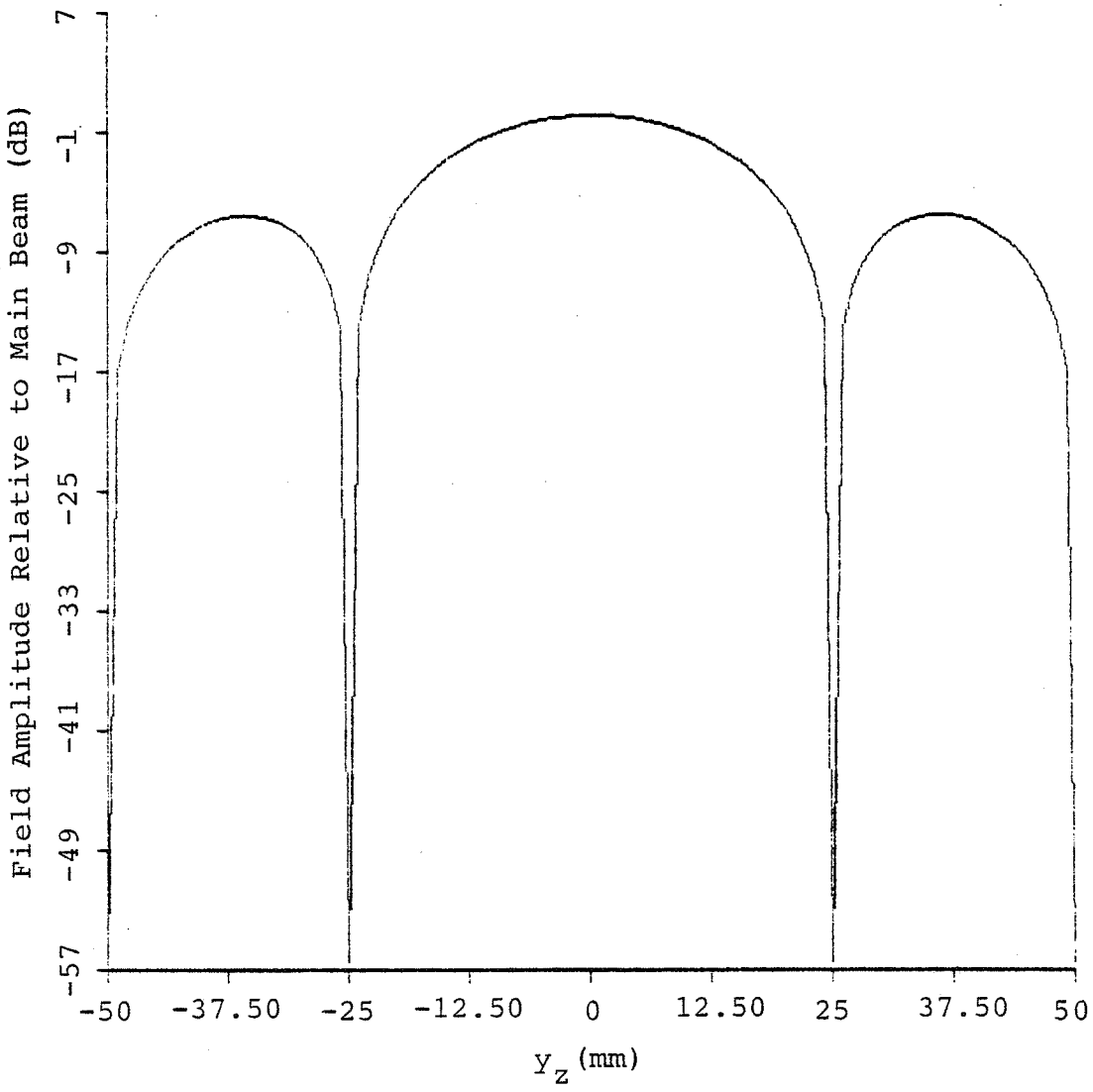

Figure 2.10. Theoretical Far Field Pattern Requiring a Mask

Number of Elements = 11

Element Width = 4.0 mm

Element Height = 30.0 mm

Element Spacing = 5.0 mm

Depth of Focus = 500.0 mm

Beam Steering = 0.0^{o}

Frequency = 1.0 MHz

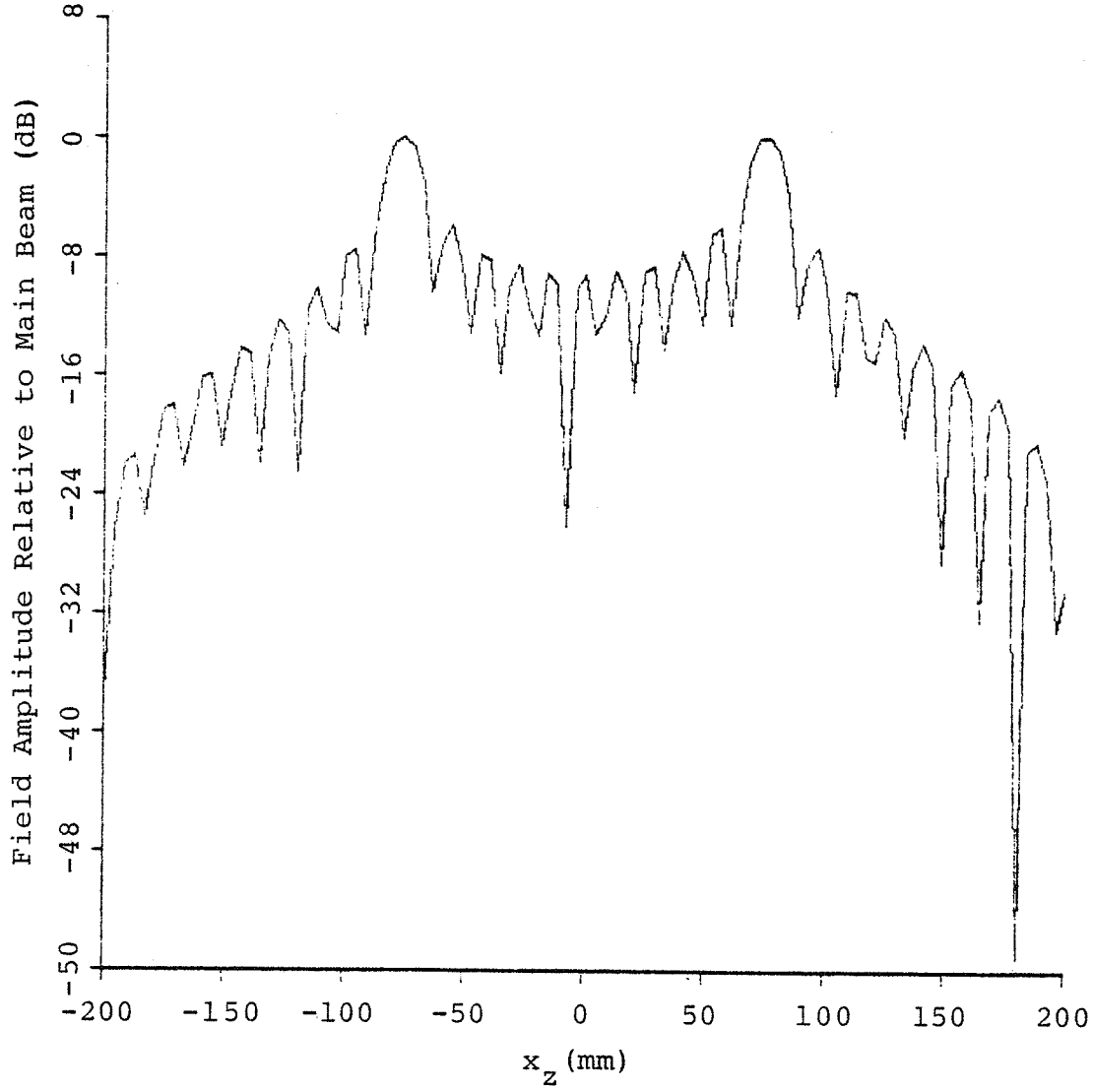

Figure 2.11. Theoretical Far Field Pattern (with Beam Steering) Requiring a Mask

Number of Elements = 11

Element Width = 4.0 mm

Element Height = 30.0 mm

Element Spacing = 5.0 mm

Depth of Focus = 500.0 mm

Beam Steering = 8.5°

Frequency = 1.0 MHz

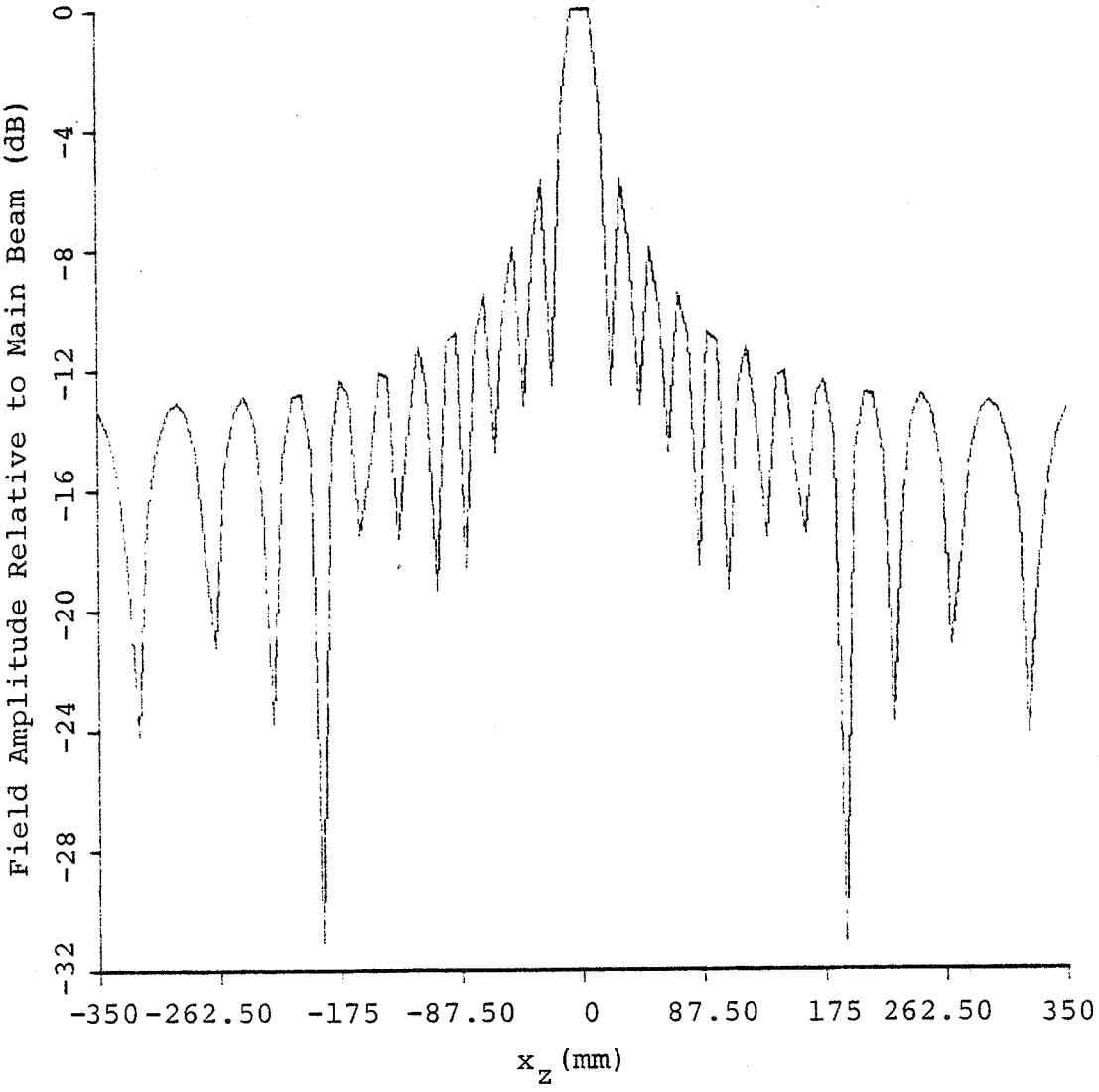

Figure 2.12. Theoretical Far Field Pattern

Number of Elements = 15

Element Width = 1.0 mm

Element Height = 18.0 mm

Element Spacing = 1.5 mm

Depth of Focus = 300.0 mm

Beam Steering = 0.0°

Frequency = 1.0 MHz

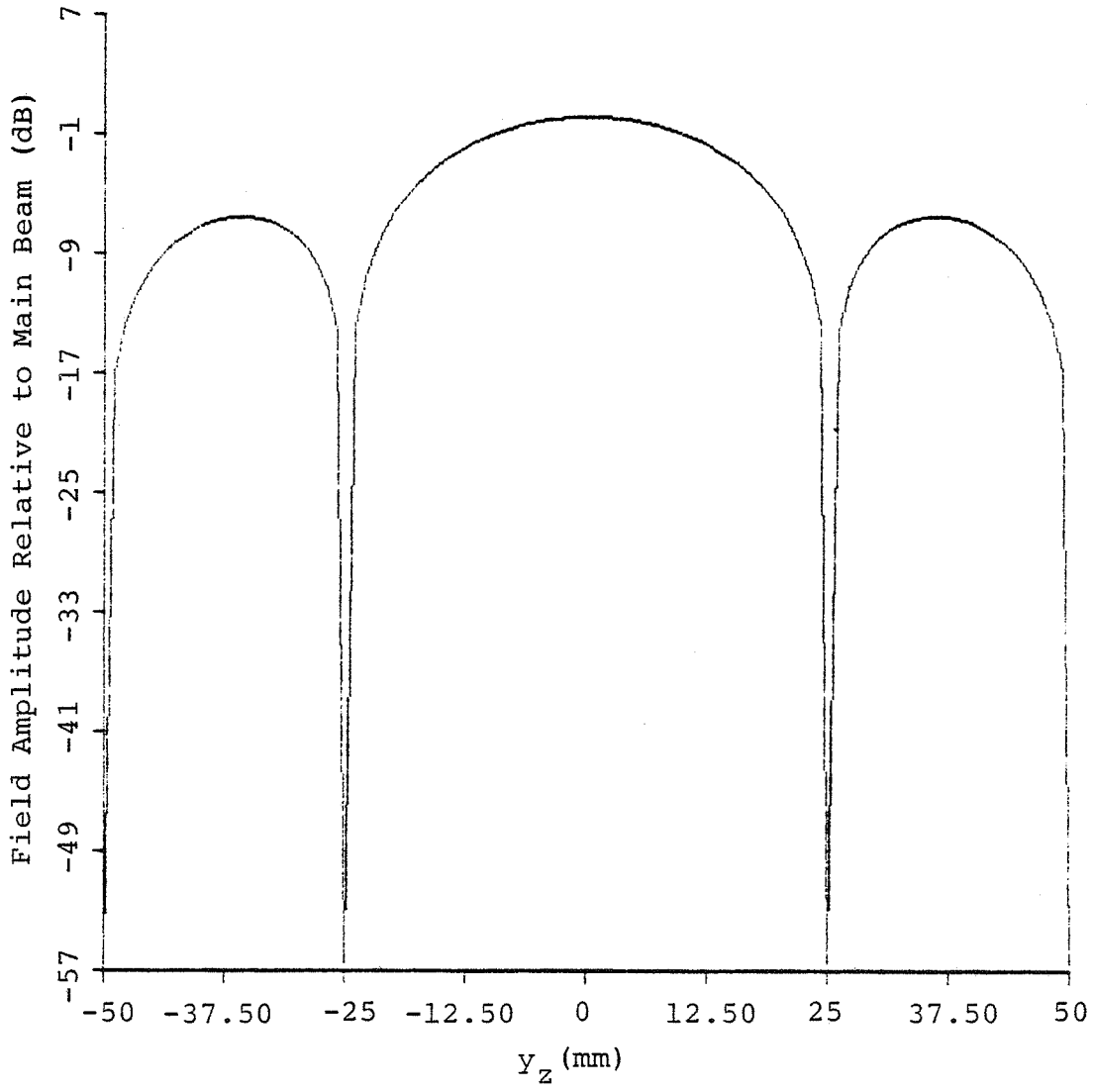

Figure 2.13. Theoretical Far Field Pattern

Number of Elements = 15

Element Width = 1.0 mm

Element Height = 10.0 mm

Element Spacing = 1.5 mm

Depth of Focus = 300.0 mm

Beam Steering = 0.0°

Frequency = 1.0 MHz

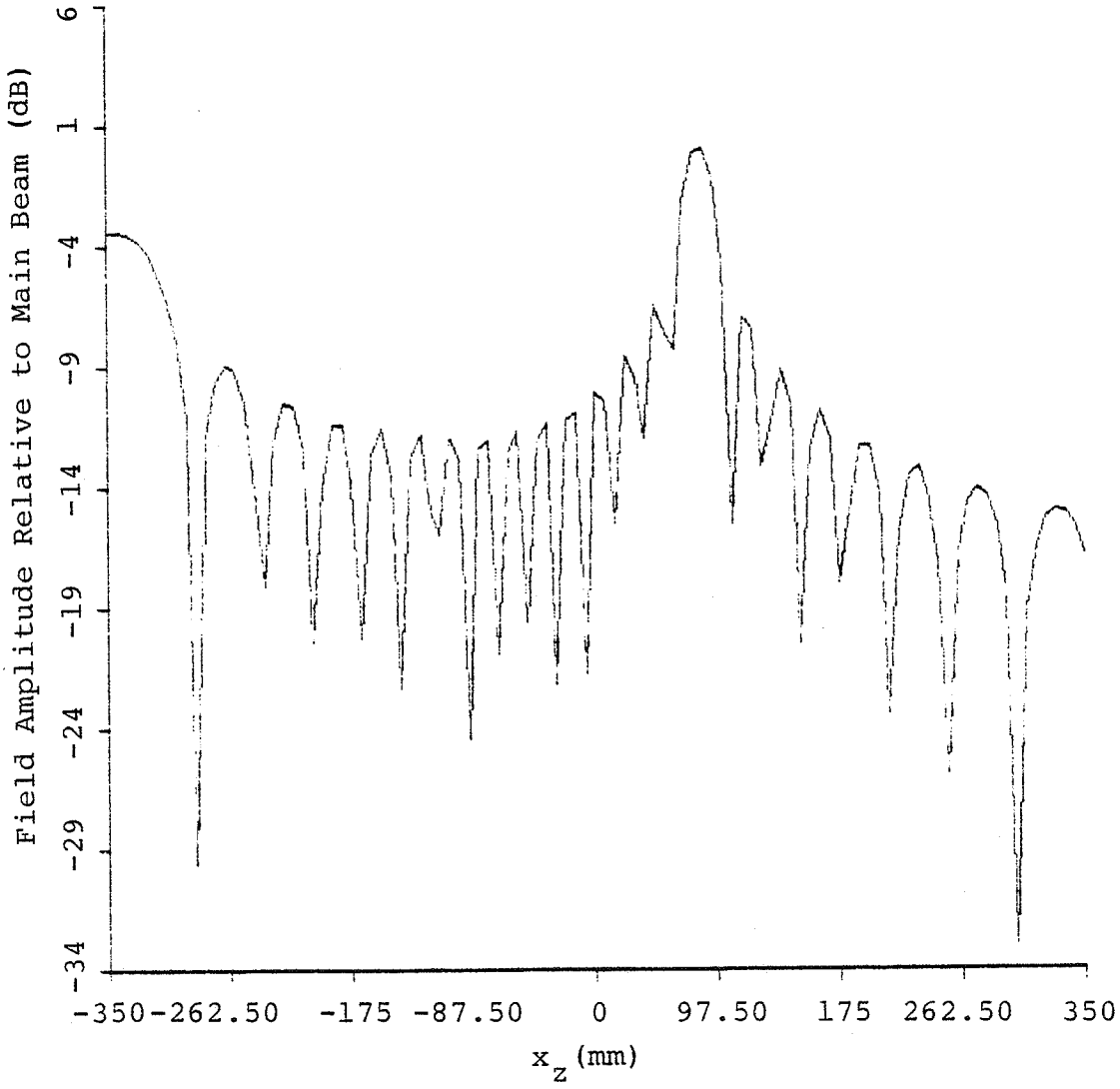

Figure 2.14. Theoretical Far Field Pattern (with Beam Steering)

Number of Elements = 15

Element Width = 1.0 mm

Element Height = 18.0 mm

Element Spacing = 1.5 mm

Depth of Focus = 300.0 mm

Beam Steering = 14.0°

Frequency = 1.0 MHz

CHAPTER III

INSTRUMENTATION

3.1. Array Construction

A linear array was constructed in order to compare the actual and theoretical field patterns. The piezoelectric material used to make the array was a three inch Channel 5400 ceramic disc resonant at 698 kHz. The element electrodes were evaporated onto the disc through a mask and consisted of a 2500 A layer of gold on a 500 A layer of chromium. The array consisted of seven 50 mm by 2 mm elements, with 1 mm spacing between the elements. Leads were attached to the electrodes using conductive epoxy. Figure 3.1 shows opposite sides of two electroded arrays. The ceramic disc was then placed in a stainless steel housing (Figs. 3.2 and 3.3) and the leads were soldered to BNC connectors inside the housing. Coaxial cables approximately 5 m long were used to connect the array elements to the digital phase shifting network.

3.2. Phase Shifting Network Design

The purpose of the phase shifting network is to produce signals to drive the elements of the linear array with the proper phases in order to achieve the desired focal spot location. A digital phase shifting network was constructed using programmable counters to achieve the desired phase shifts. Each array element is driven by a counter group. Figure 3.4 shows a block diagram of the network. The whole network is controlled via a Perkin Elmer 7/32 minicomputer which provides 12 bits of encoded data to Vaughn's Interface (Vaughn, 1981). The upper four bits are

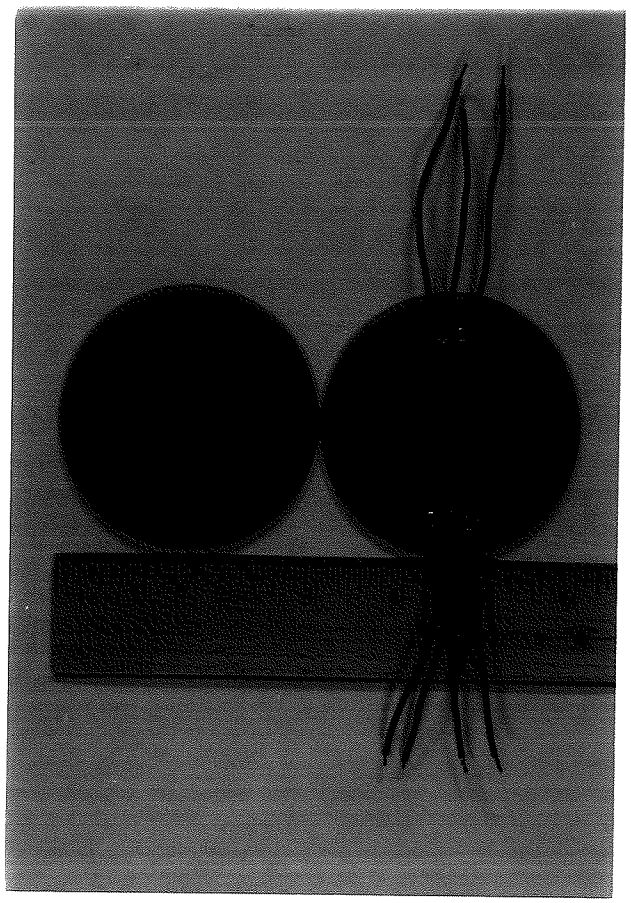

Figure 3.1. Opposite Sides of Two Electroded Arrays

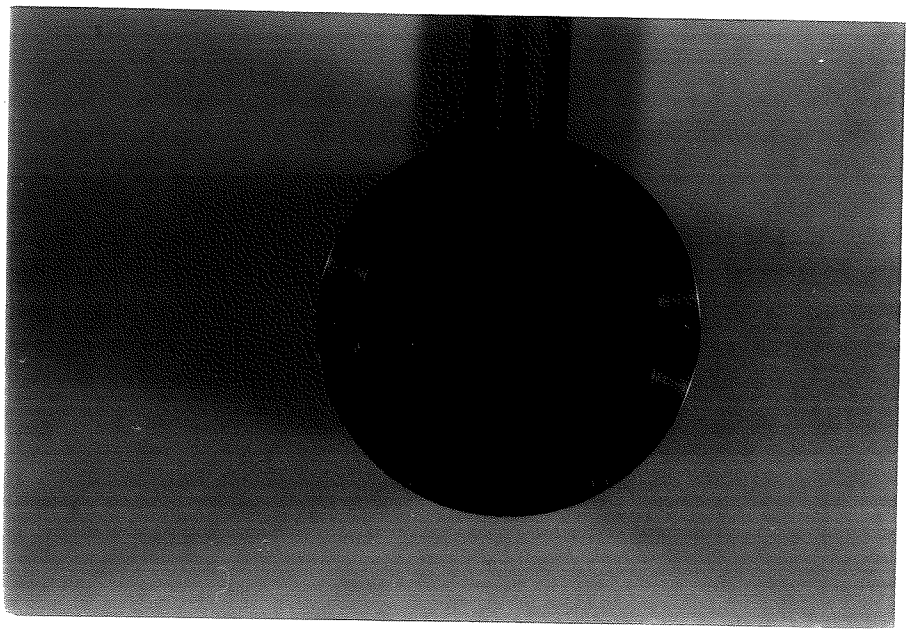

Figure 3.2. Array Housing (Front View)

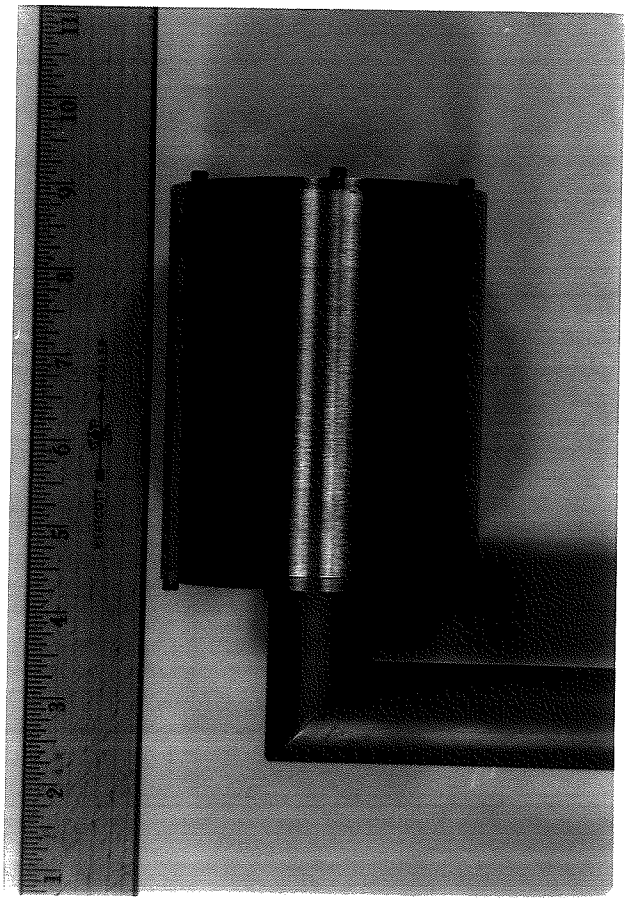

Figure 3.3. Array Housing (Side View)

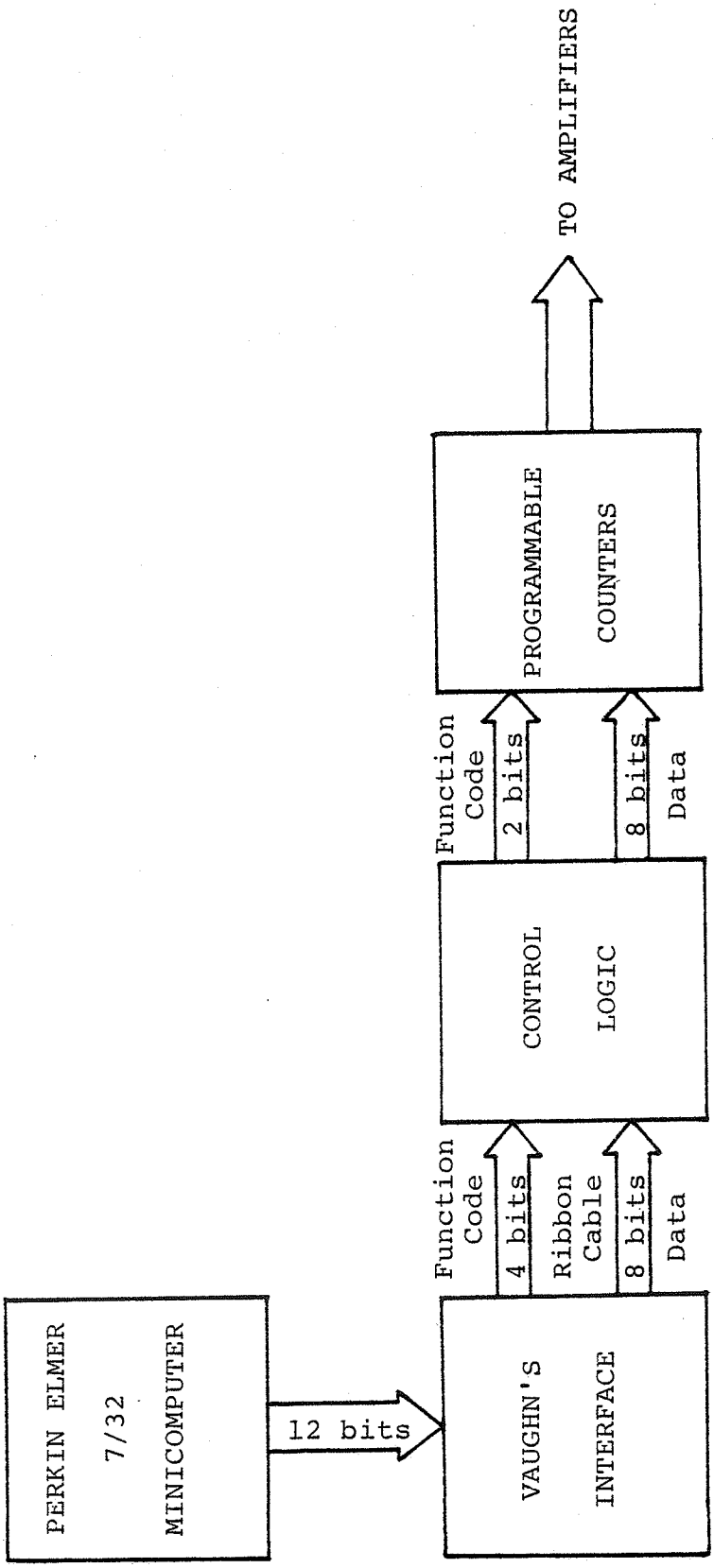

Figure 3.4. Digital Phase Shifting Network

decoded into 16 function codes of which four are used by the phase shifting network. These four function codes and the lower eight bits of the encoded data contain the information needed to program the phase and amplitude of a counter group. The data bits contain either the address of the counter group to be programmed, or the number to be programmed into the counter group. The Control Logic interprets the function codes to determine which operation is to occur. The Control Logic can start, stop, or load the programmable counters depending on the status of the function codes.

The signal to each array element is generated by the counter group, which consists of two sets of emitter coupled logic (ECL) counters. Each set contains two cascaded four bit counters set up in a divide by 128 mode. The clock signal input to the counters is 128 times the desired operating frequency of the array element. These high operating frequencies made it necessary to use high speed emitter coupled logic. Since the maximum frequency at which the ECL counters can operate is about 120 MHz (MECL 10K series), the maximum operating frequency of the array is about 1 MHz.

The most significant bit of each output of the two sets of counters is applied to an input of an AND gate (10104). The resulting output of the AND gate is a pulsed waveform which is filtered and amplified to drive an element of the array.

The amplitude and phase of the signal driving an array element are controlled by programming the two sets of counters in the counter group for various initial counter states. Figure 3.5 illustrates how this is accomplished. The amplitude is changed by changing the duty cycle of the output of the AND gate which can be

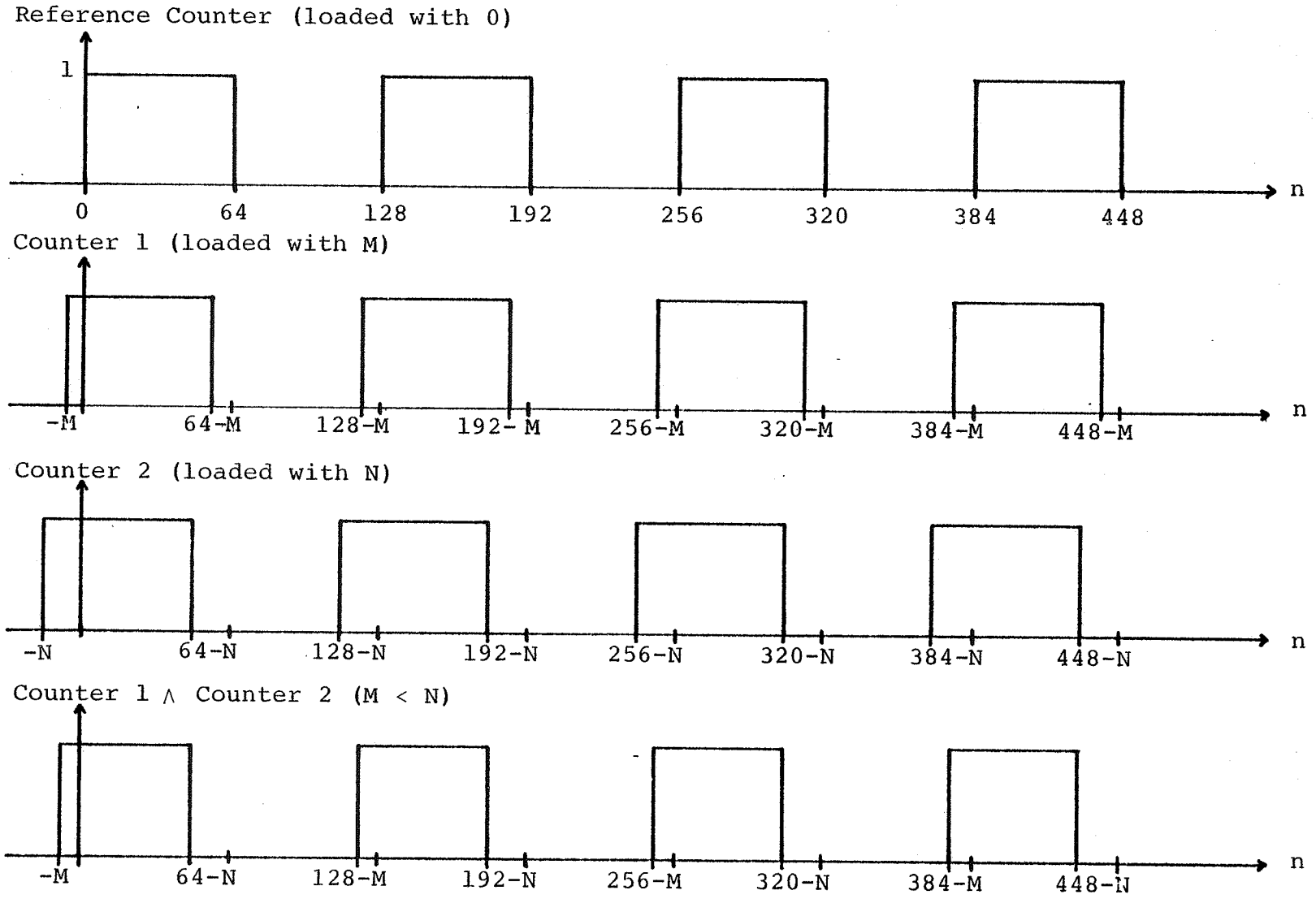

Figure 3.5. Counter Programming Example

controlled by varying the initial states between the two sets of counters in the counter group. The phase is controlled by varying the initial states between counter groups. The amplitude and phase of the fundamental frequency of the output of the AND gate (where $\wedge$ represents the AND operation) for the case M < N :

$$A = K \int_{-64}^{64} [\text{Counter 1} \wedge \text{Counter 2}] e^{-j\frac{2\pi n}{128}} dn \quad . \qquad (3.1)$$

Completing the integral yields

$$A = -K' \left[e^{-j\frac{2\pi(64-N)}{128}} - e^{+j\frac{2\pi M}{128}} \right] \qquad (3.2)$$

where M and N are the values loaded into the counters, and

$$K' = K\left(\frac{128}{-j2\pi}\right)$$

Since

$$e^{-j\frac{2\pi(64-N)}{128}} = -e^{j\frac{2\pi N}{128}}$$

Eq. 3.2 can be simplified to give

$$A = K' \left[e^{j\frac{2\pi}{128}\left(\frac{N+M}{2}\right)} \right] \left[e^{j\frac{2\pi}{128}\left(\frac{N-M}{2}\right)} + e^{-j\frac{2\pi}{128}\left(\frac{N-M}{2}\right)} \right] \quad . \qquad (3.3)$$

Multiplying the two terms in Eq. 3.3 yields

$$A = 2K' \left[e^{j\frac{2\pi}{128}\left(\frac{M+N}{2}\right)} \right] \left[\cos\frac{2\pi}{128}\left(\frac{N-M}{2}\right) \right] \quad . \qquad (3.4)$$

Since only the relative amplitude is of interest when programming the counters, the constant 2K' can be dropped from Eq. 3.4. This gives

$$\text{Relative Amplitude} = \cos\frac{2\pi}{128}\left(\frac{N-M}{2}\right) \quad . \tag{3.5}$$

From Eq. 3.4 it can also be seen that the phase angle relative to a reference counter with M and N equal to zero is given by

$$\text{Phase Angle} = \frac{2\pi}{128}\left(\frac{M+N}{2}\right) \text{ rads} \quad . \tag{3.6}$$

Reversing the roles of M and N has no effect on the relative amplitude and phase, hence the case for N > M will give the same result. The maximum phase error possible is 2.8125^{o} using the counters in a divide by 128 mode. Driving signals with frequencies up to about 2 MHz could be produced if the counters were set up in a divide by 64 mode. However, this would result in a doubling of the maximum possible phase error for each element which would lead to a loss in sharpness of the array focus. The program used to control the phase shifting network of the array is listed in Appendix.

3.3. Circuit Description

The circuit board diagrams for the phase shifting network are shown in Figs. 3.6 through 3.9. Figures 3.6, 3.8, and 3.9 constitute the Control Logic portion of the phase shifting network referred to in Sec. 3.1. Board 1 (Fig. 3.6) receives its inputs from the Interface through a 24 conductor ribbon cable. The four function codes, $\overline{\text{FUNC 10}}$ - $\overline{\text{FUNC 13}}$, are first passed through a TTL

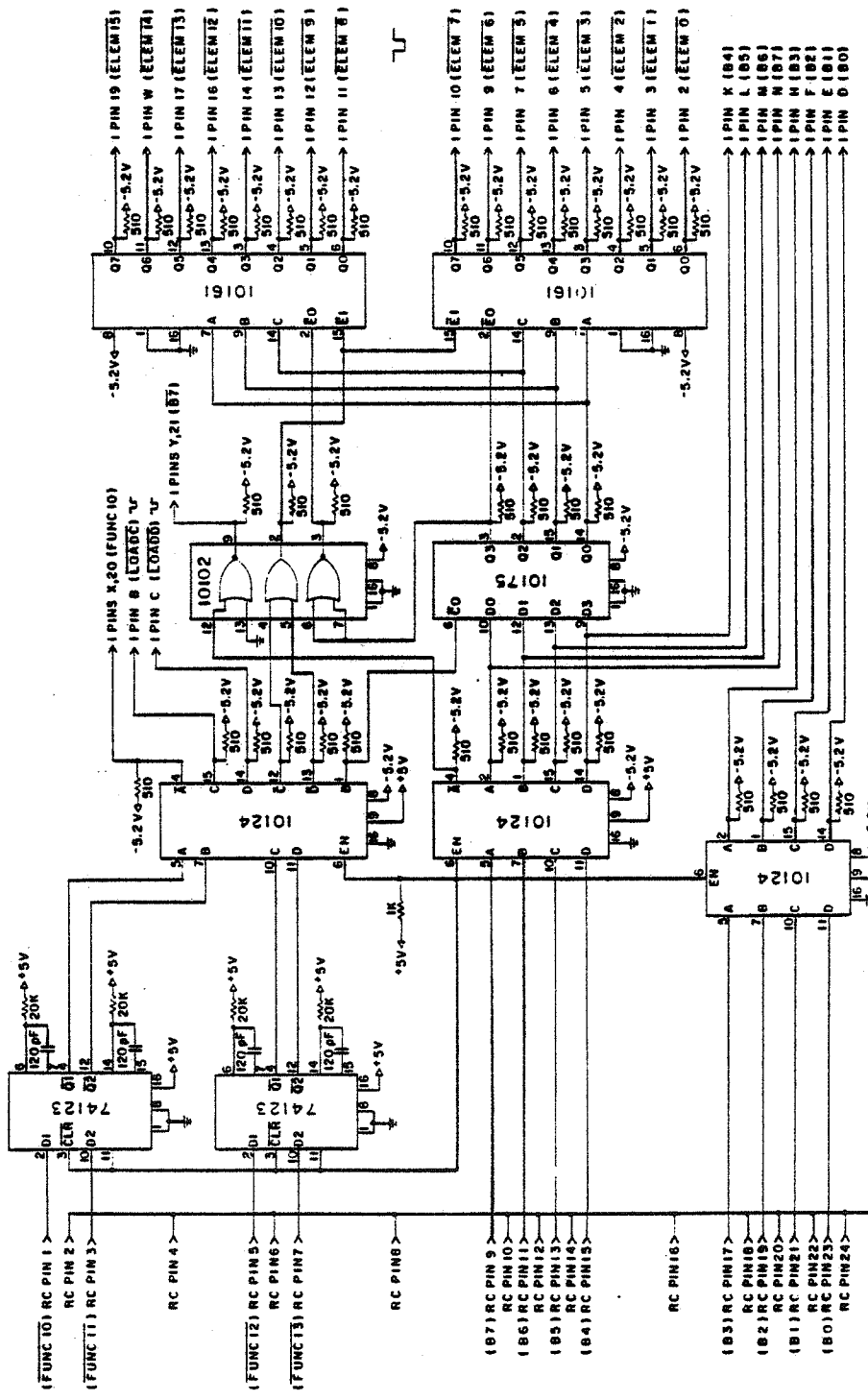

Figure 3.6. Board 1

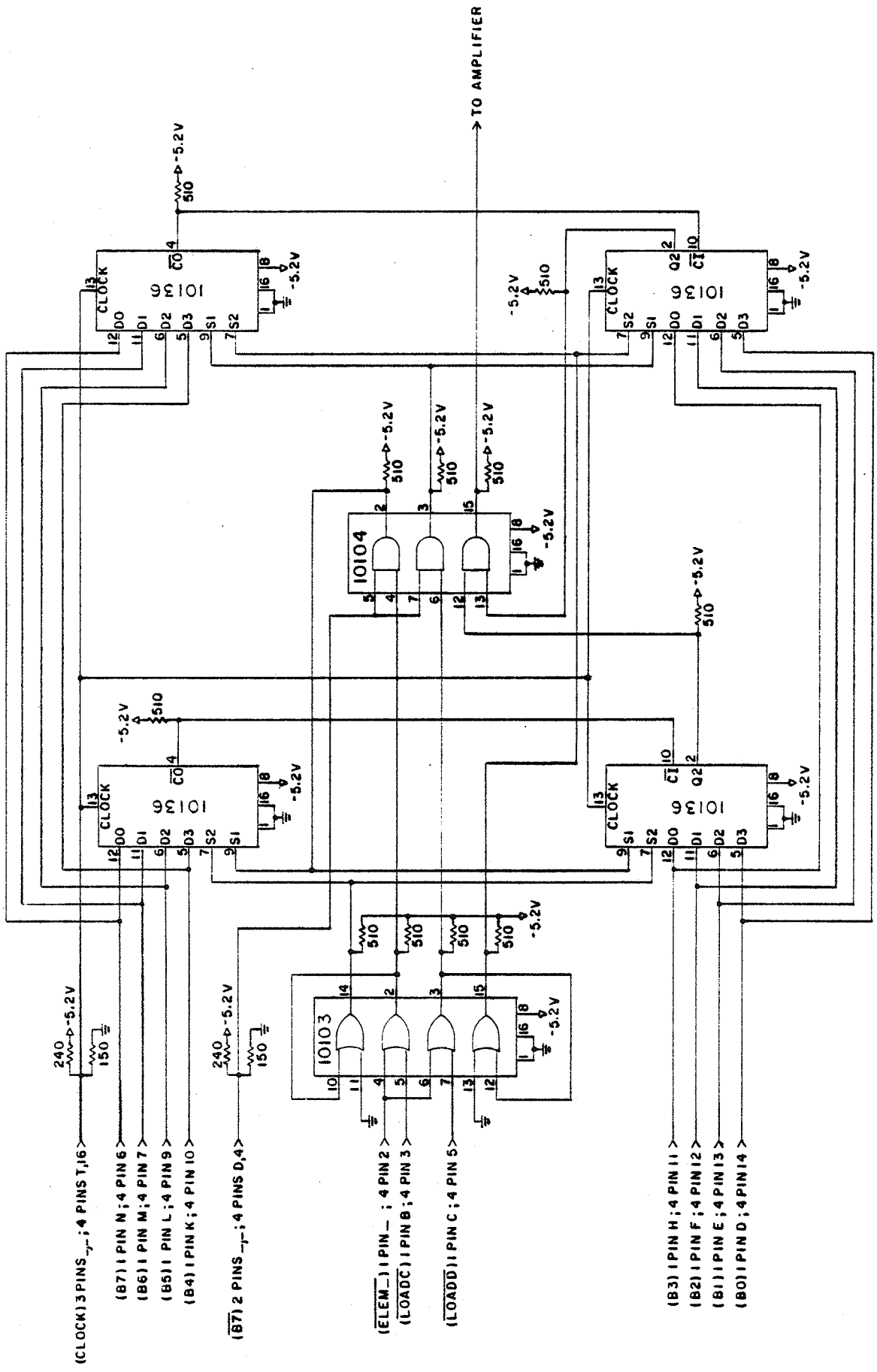

Figure 3.7. Boards 2A - 2G

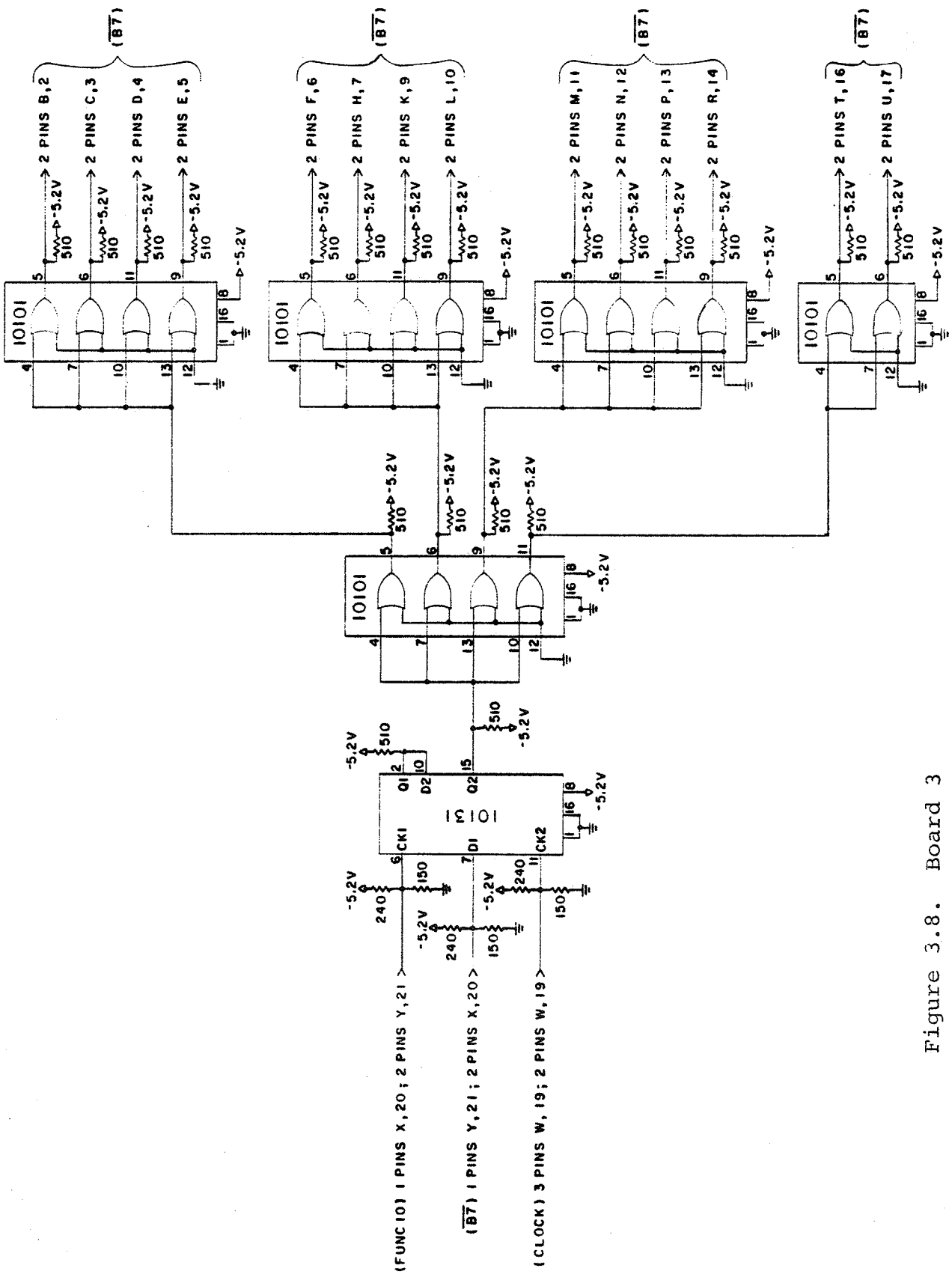

Figure 3.8. Board 3

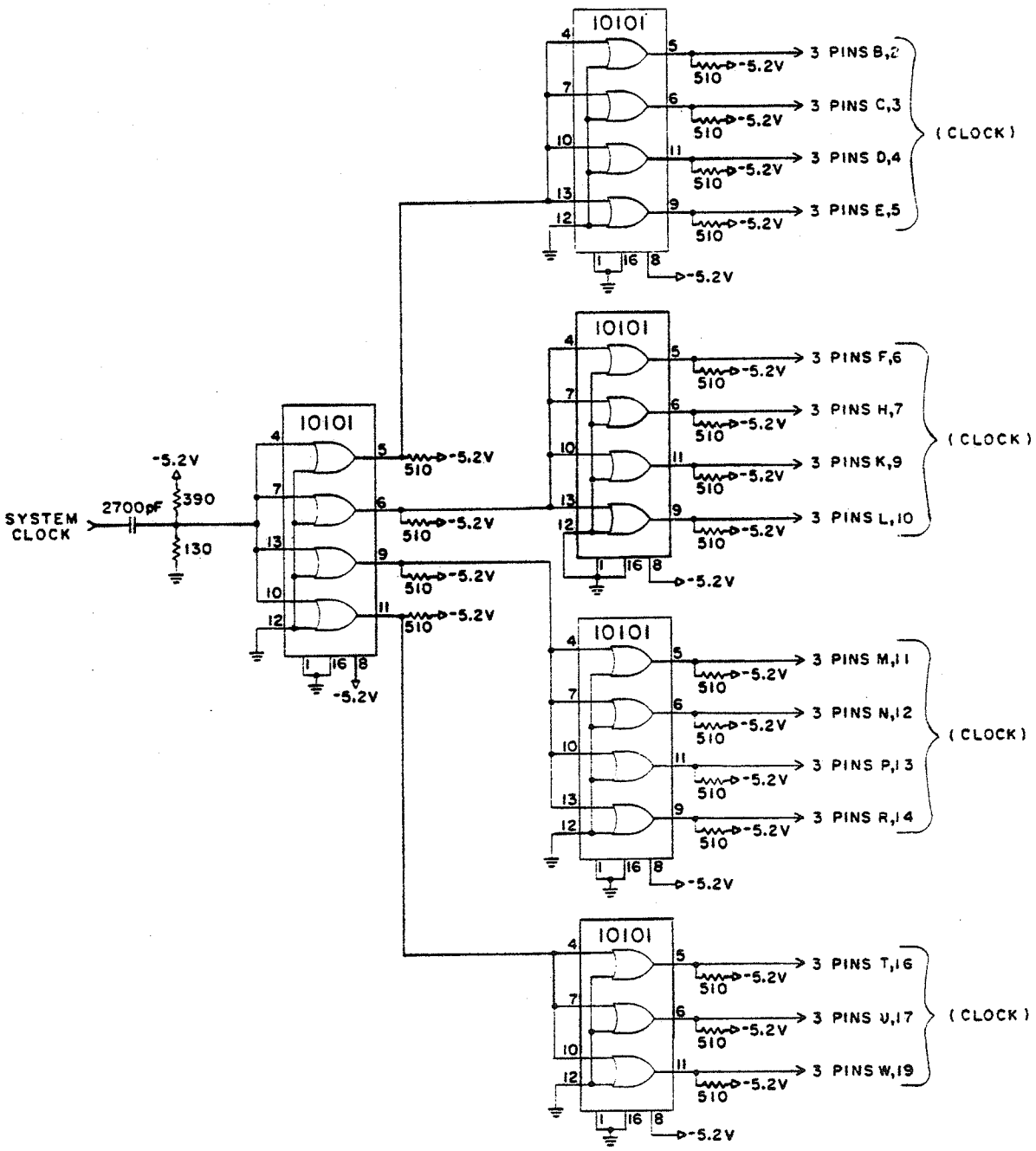

Figure 3.9. Board 4

monostable multivibrator (74123) which prevents bouncing on transitions. Since Vaughn's Interface and the multivibrators use TTL logic, TTL to ECL translators (10124) are used for all inputs. When $\overline{\text{FUNC 11}}$ is low, the lower four data bits, B7 - B4, contain the information specifying which counter group is to be programmed. These four bits are then loaded into the 4 bit latch (10175). The 4 bit latch feeds a 4 to 16 decoder (constructed with two 3 to 8 decoders; 10161) to select one of the counter group boards, Boards 2A - 2G (Fig. 3.7). The outputs of the decoders, $\overline{\text{ELEM 0}}$- $\overline{\text{ELEM 15}}$, are fed to the counter group of each element. A low on $\overline{\text{ELEM 0}}$ through $\overline{\text{ELEM 15}}$ indicates which counter group is to be loaded. The outputs, B0 - B7, of the translators are fed to all counters and provide the data to program the counters. The outputs, $\overline{\text{LOADC}}$ and $\overline{\text{LOADD}}$, from the translator, are fed to each counter group board. A low on one of the outputs $\overline{\text{ELEM 0}}$ through $\overline{\text{ELEM 15}}$ indicates which counter group is to be loaded. A low on $\overline{\text{LOADC}}$ or $\overline{\text{LOADD}}$ indicates which set of counters in the counter group is to be loaded. Data bit $\overline{\text{B7}}$ controls the starting and stopping of the counters. A low on $\overline{\text{B7}}$ will start all of the network's counters, and a high will stop them. Since $\overline{\text{B7}}$ will be driving several gates, the circuit on Board 3 (Fig. 3.8) is used to extend $\overline{\text{B7}}$ to be able to drive up to 14 gates. The circuitry on Board 4 (Fig. 3.9) provides all the boards with a clock signal. The system clock used to drive this board is an external signal generator. When the final design frequency has been chosen, an oscillator of the proper frequency will be used in place of the signal generator.

3.4. Amplifier Design

The amplifiers used to drive the elements of the array were designed to provide each element with about 250 mW of power. Ultimately all amplifiers combined will have to supply enough power to the array to provide 300 W of acoustical power to ensure proper heating in reasonable lengths of time. This will require the amplifiers produce more than 300 W of electrical power since the efficiency of the elements will be less than 100%. Since this initial design was intended to be used only to measure the far field patterns produced by the array, 250 mW per element was sufficient.

Figure 3.10 shows the final amplifier design circuit. The 470 μH inductor and 100 pF capacitor combination at the input is a filter allowing only the frequency of interest (698 kHz) to pass unattenuated. The first stage of the amplifier uses a 2N2222 general purpose transistor. This stage is used to isolate the emitter coupled logic from the second stage of the amplifier. This isolation prevents loading of the emitter coupled logic. The 100Ω trimming potentiometer in the emitter lead of the 2N2222 is a gain control which is of particular importance. Since each element has a slightly different impedance, the voltage across each element will have to be adjusted by potentiometer to ensure that each element provides the the same power level. The second stage of the amplifiers uses a 2N2270 power transistor that is capable of dissipating up to 1 W of power. Due to matching considerations, the maximum power this amplifier can deliver to an element is about 250 to 350 mW depending on the impedance of the element. The matching transformer in the collector lead of the

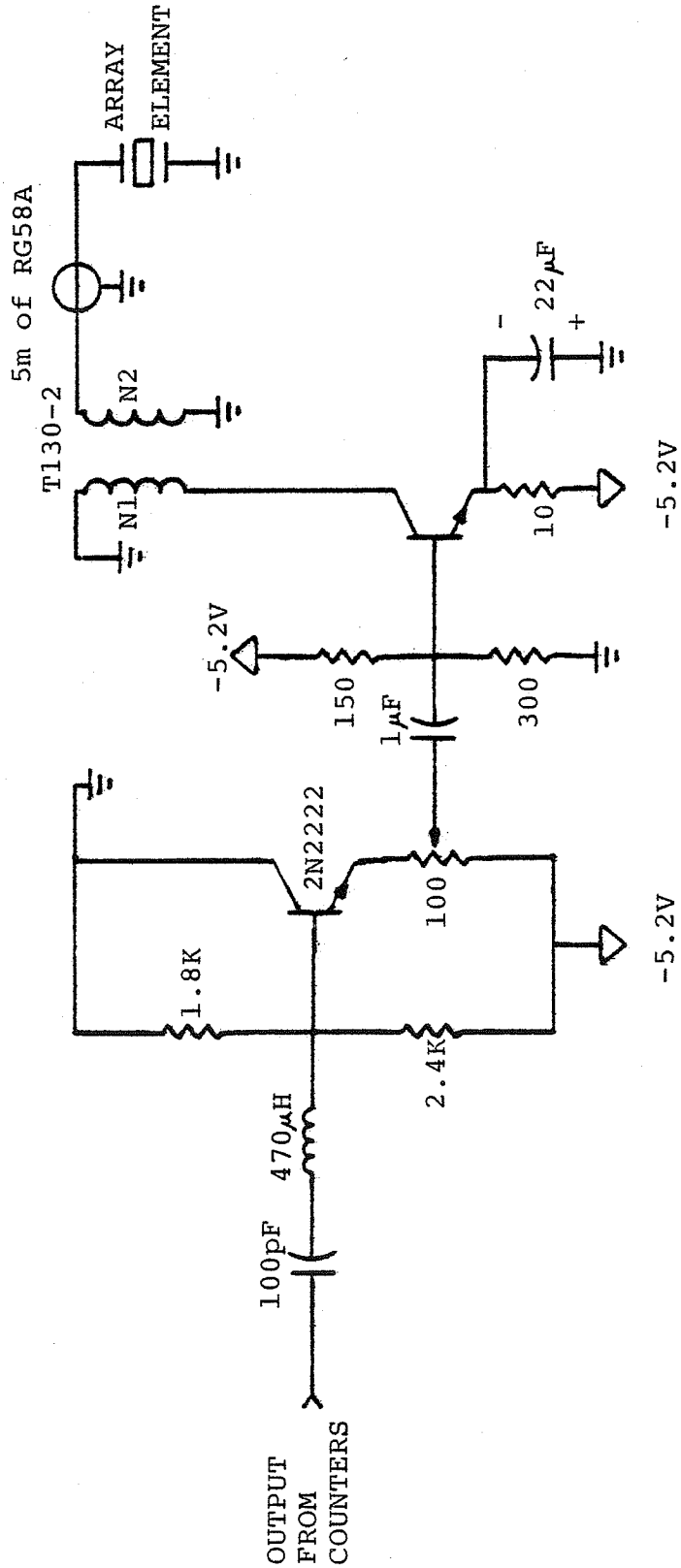

Figure 3.10. Amplifier Circuit Diagram

2N2270 allows maximum power transfer without saturating the driving transistor. The secondary's parallel inductance was selected to cancel out the element's capacitive reactance. Table 3.1 lists the impedance of each of the seven elements and cable, transformer windings, and the voltage necessary across each element to ensure that they are all operating at the maximum possible power level. The elements are numbered in the order they appear from left to right in the array.

Table 3.1. Amplifier Matching Data

Element	Impedance (ohms)	N1 (turns)	N2 (turns)	V_{max} (volts RMS)
0	$163 \angle -42^{\circ}$	24	71	7.6
1	$179 \angle -44^{\circ}$	25	73	8.1
2	$196 \angle -54^{\circ}$	24	71	9.4
3	$195 \angle -56^{\circ}$	24	70	9.6
4	$195 \angle -52^{\circ}$	24	71	9.2
5	$180 \angle -44^{\circ}$	25	73	8.1
6	$161 \angle -44^{\circ}$	23	68	7.7

CHAPTER IV

RESULTS

4.1. Test Setup

The array transducer was placed in a tank filled with degassed water and a hydrophone probe was used to measure the far field patterns of the array. The hydrophone probe was swept across the field of the transducer array at the desired depth of focus. The output of the hydrophone probe was amplified and fed to a true RMS voltmeter. By referencing the voltmeter to the point of maximum intensity in the field pattern, the output of the voltmeter indicated the intensity in decibels of the field pattern relative to that point.

4.2. Test Results

The far field patterns for two focal lengths with and without beam steering were measured. In Figs. 4.1 through 4.4 these field patterns are compared with the theoretical field patterns. This comparison shows that the measured main beam is much broader and is not steered as far as the theory predicts. The actual grating lobes are much further down in intensity than predicted by theory.

There are several possible explanations for the discrepancies between the actual and theoretical results. The phase shifting network has a maximum possible error of 2.8125° per element which would cause the main beam to be broader since the focus would not be as sharp. A much greater problem than the phase shift error was the coupling between the elements of the array. This coupling

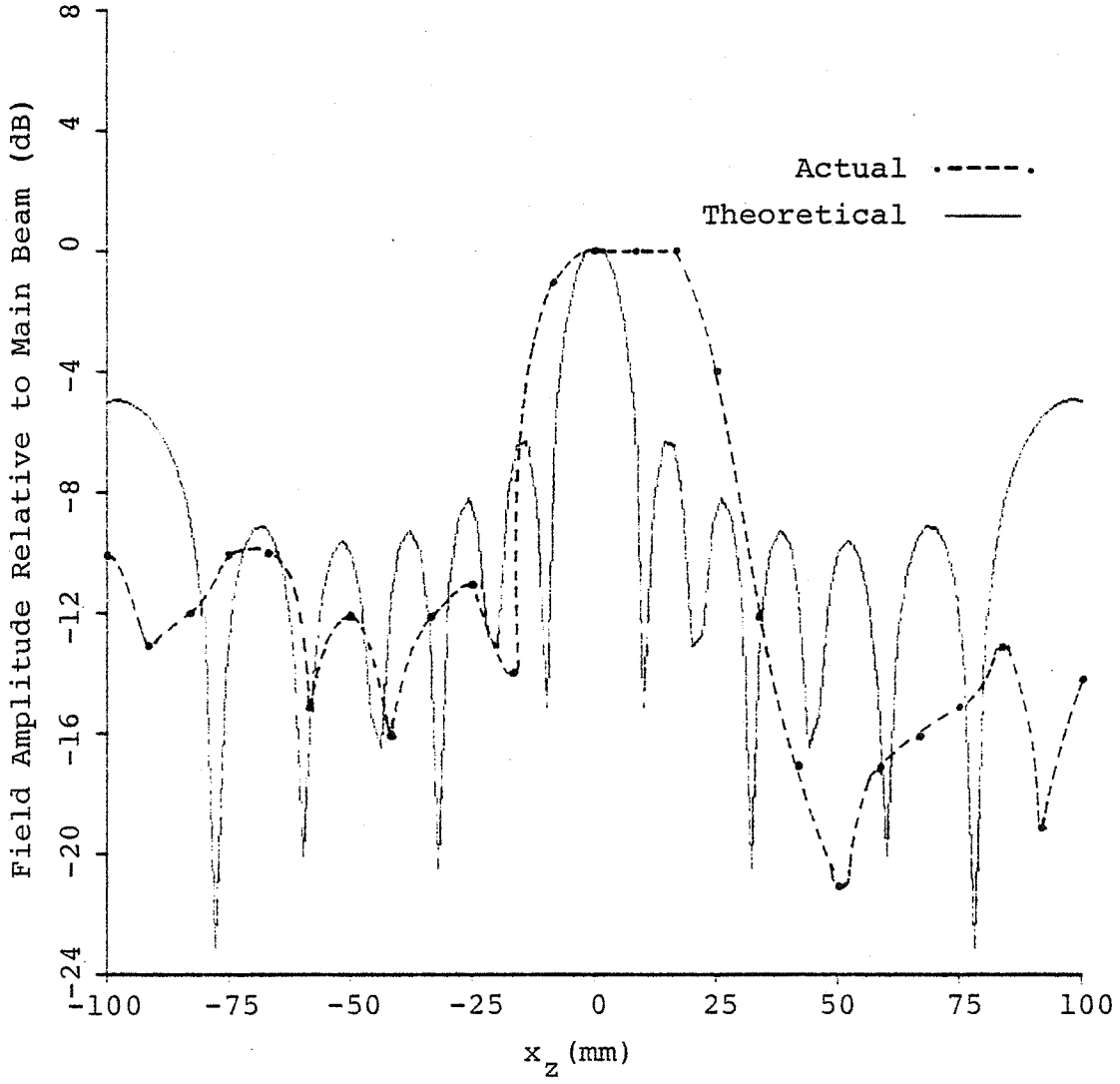

Figure 4.1. Actual and Theoretical Far Field Patterns

Number of Elements = 7

Element Width = 2.0 mm

Element Height = 50.0 mm

Element Spacing = 3.0 mm

Depth of Focus = 100.0 mm

Beam Steering = 0.0°

Frequency = 698.0 kHz

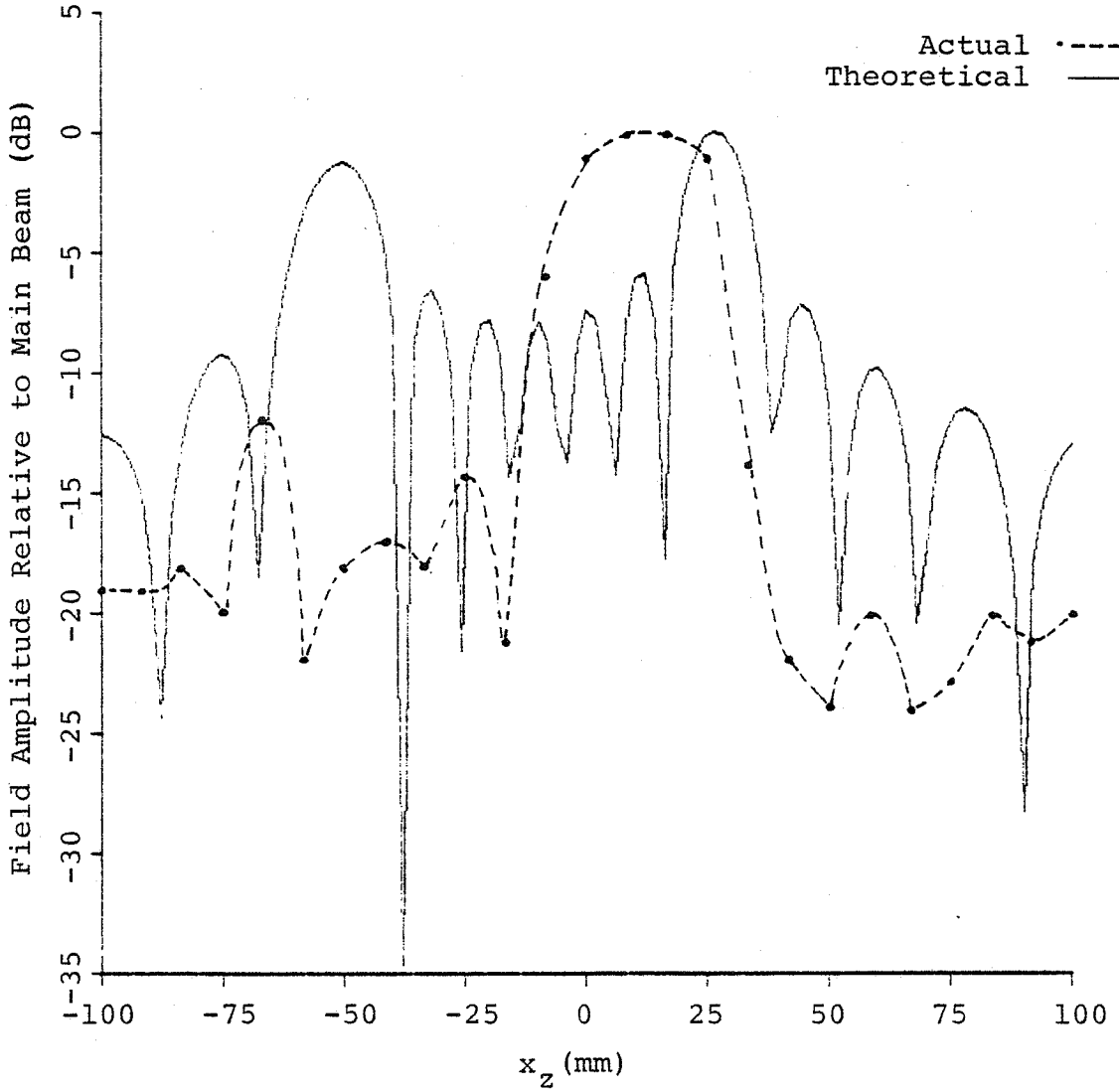

Figure 4.2. Actual and Theoretical Far Field Patterns (with Beam Steering)

Number of Elements = 7

Element Width = 2.0 mm

Element Height = 50.0 mm

Element Spacing = 3.0 mm

Depth of Focus = 100.0 mm

Beam Steering = 15.0°

Frequency = 698.0 kHz

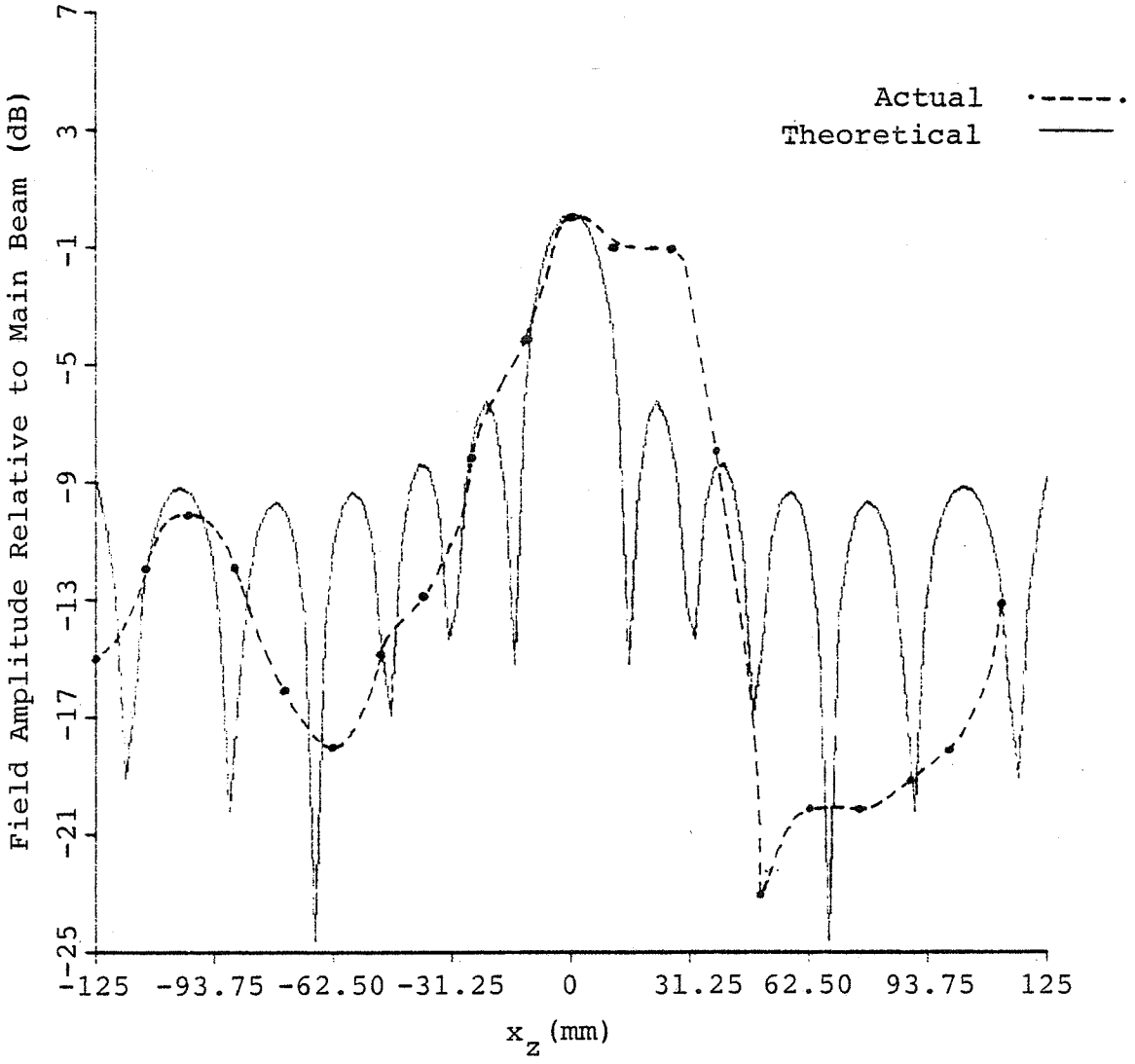

Figure 4.3. Actual and Theoretical Far Field Patterns

Number of Elements = 7

Element Width = 2.0 mm

Element Height = 50.0 mm

Element Spacing = 3.0 mm

Depth of Focus = 150.0 mm

Beam Steering = 0.0°

Frequency = 698.0 kHz

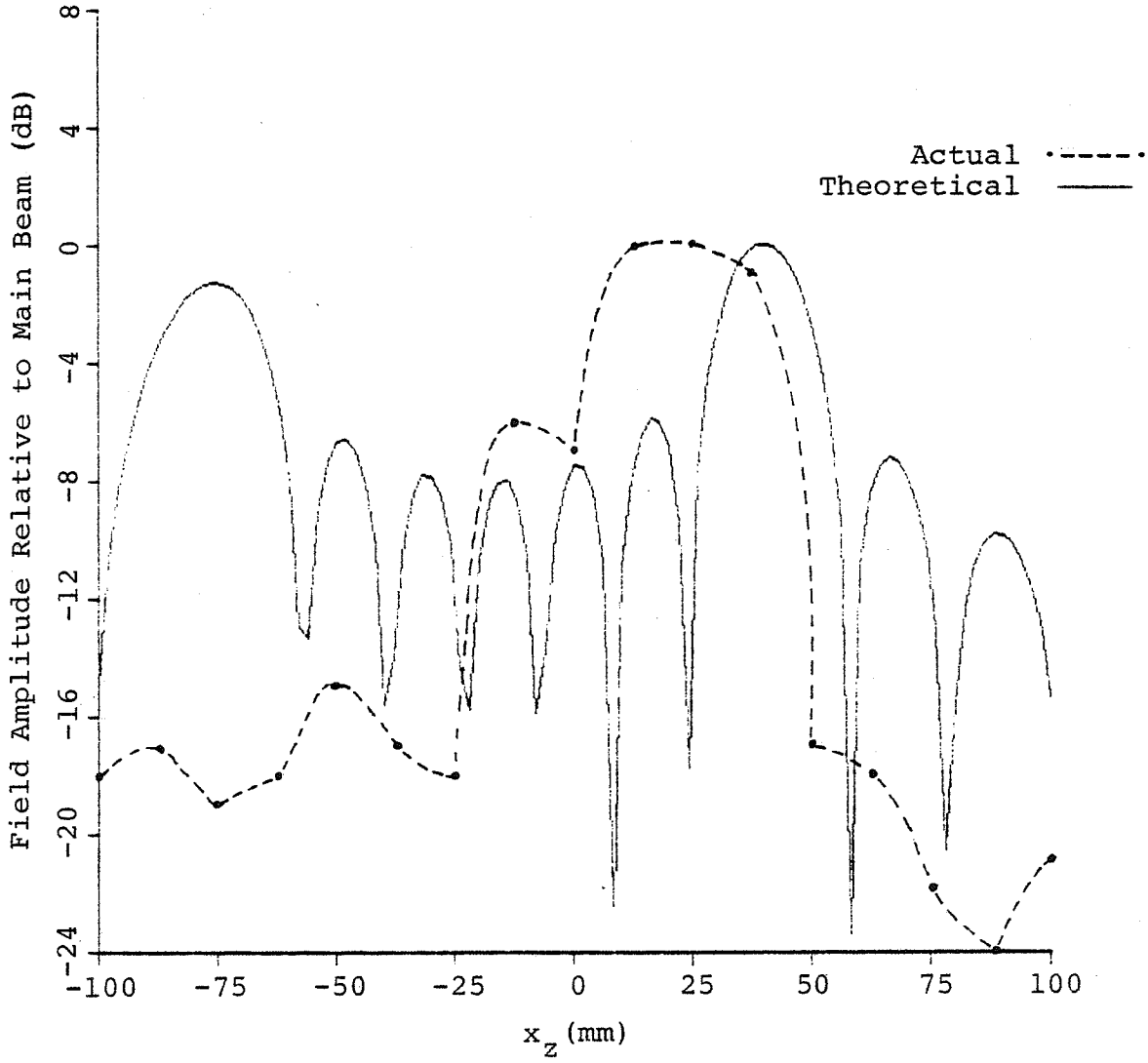

Figure 4.4. Actual and Theoretical Far Field Patterns (with Beam Steering)

Number of Elements = 7

Element Width = 2.0 mm

Element Height = 50.0 mm

Element Spacing = 3.0 mm

Depth of Focus = 150.0 mm

Beam Steering = 15.0°

Frequency = 698.0 kHz

was either electrical or acoustical in nature. Acoustical coupling could have been present since the elements of the array were not physically isolated from each other. The acoustic output of any one element was transmitted to all of the other elements. This is probably the main reason for the difference between the theoretical and measured results. The possible presence of electrical coupling could not be ruled out. Figure 4.5 shows the signals present on each element for the field pattern shown in Fig. 4.1. The observed phase shifts of the signals could not be accurately measured because the signals were too distorted due to interelement coupling. Signals on the elements in the middle of the array experienced the greatest amount of distortion. Since the signals were distorted, each element was not necessarily driven by a signal with the desired phase shift. This could explain the broader main beam and lack of appropriate beam steering.

The results obtained using a spectrum analyzer to determine the harmonics present in the signals driving each element are listed in Table 4.1. These results show that the elements in the center of the array had greater harmonic distortion, particularly the half harmonic, than the elements at the ends of the array. In order to determine whether these higher harmonics and subharmonics were generated by the array or the amplifiers, a spectrum analysis of each element driven separately was performed. The results, shown in Table 4.2, show that there are no subharmonics present and that the amplitudes of the higher harmonics were far down from the fundamental. This seems to indicate that the harmonic distortion was produced by the array and not the amplifiers. The

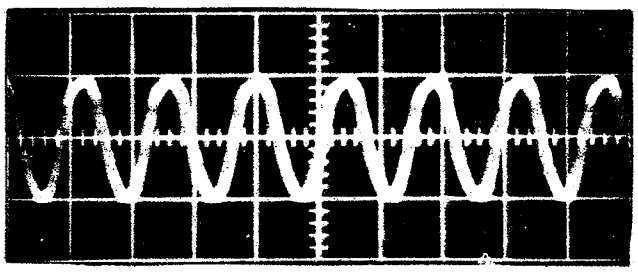

Element 0

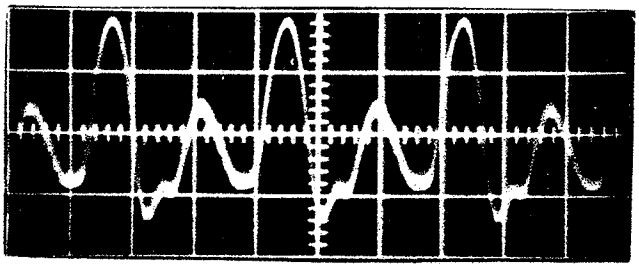

Element 1

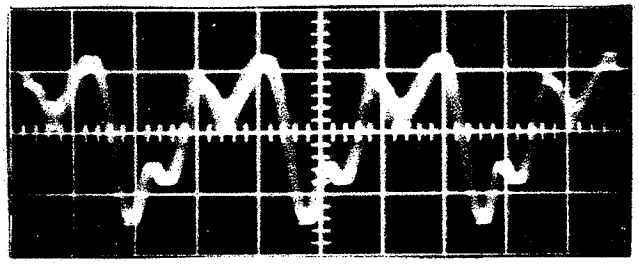

Element 2

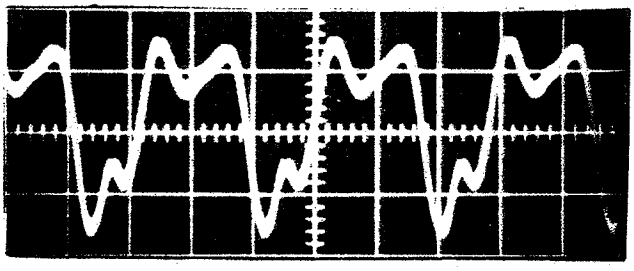

Element 3

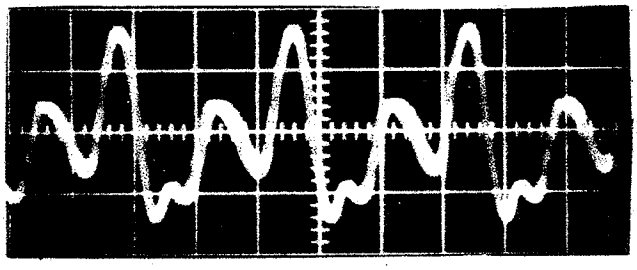

Element 4

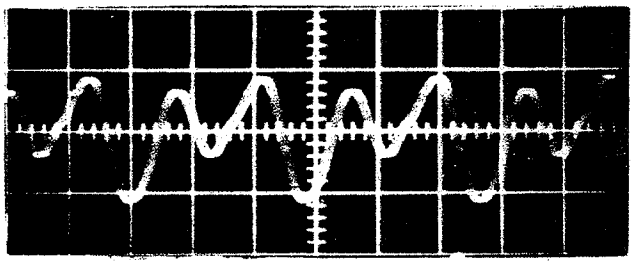

Element 5

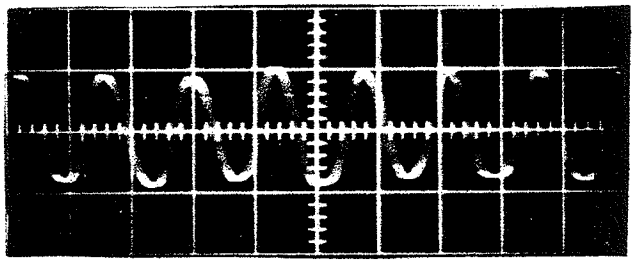

Element 6

Figure 4.5. Voltage Waveforms Across Each Element

Table 4.1. Spectrum analysis of the signals driving the elements of the array. Amplitude (dB) is referenced to f_o = 698 kHz.

	Frequency				
Element	0.5 f_o	1.5 f_o	2 f_o	2.5 f_o	3 f_o
0	-25	-25	-18	-44	-22
1	- 6	-11	-15	-22	-21
2	+ 3	- 4	- 8	-21	-22
3	+ 5	- 4	- 6	-19	-22
4	- 9	-13	-15	-22	-26
5	- 1	- 7	-14	-22	-25
6	-24	-26	-16	-40	-24

Table 4.2. Spectrum analysis of the signal driving only one element of the array. Amplitude (dB) is referenced to f_o = 698 kHz.

	Frequency		
Element	2 f_o	3 f_o	4 f_o
0	-19	-26	-34
1	-29	-24	-34
2	-23	-22	-36
3	-21	-21	-34
4	-25	-21	-33
5	-20	-30	-44
6	-23	-24	-40

spectrum analyzer was also used to examine the harmonics in the signal received from the hydrophone probe when placed in the beam focus. The results showed that the harmonics and subharmonics were reduced more than 30 dB from the fundamental.

4.3. Conclusions

The difference between the observed and theoretical field patterns was not unusual considering the level of interelement coupling present. The cross coupling between elements can lead to a decrease in range resolution, and cause an increase in rolloff with the angle θ (Dias, 1982). The increase in rolloff causes the amplitude of the grating lobes to be decreased. This decrease in grating lobe amplitude was observed in the measured field patterns which also exhibited the decreased resolution in the form of a broader main beam.

CHAPTER V

RECOMMENDATIONS FOR FUTURE WORK

5.1. Acoustical Coupling

The array elements should be acoustically decoupled from each other. This can be accomplished by cutting grooves between the elements or using individual elements mounted on some kind of lossy backing material. The optimum depth of a groove should be determined considering the structural integrity of the ceramic and the level of acoustical decoupling.

5.2. Maximum Power Levels

The amount of power that an element of a given size can handle before failure needs to be determined because the number and size of the elements in the final design will depend on how much power they can handle. In addition, the type of failure that occurs when too much power is applied should be determined. If the failure is associated with the bonding of the electrode to the ceramic, would a different type or thickness of electrode solve the problem? If the failure is with the bonding of the lead to the electrode, can a different type of bonding be used to solve the problem?

5.3. Near Field Focusing

Theoretical equations that describe focusing and beam steering in the near field need to be implemented on the computer. If focusing can be achieved with appropriate beam steering in the near field, then perhaps larger elements (greater on-center spacing) can be used for shorter depths of focus.

5.4. Array Geometries

Alternate array geometries should be studied to determine if they could provide adequate focusing and beam steering while using fewer elements than the linear array approach. Theoretical field patterns would have to be computed for these alternate array geometries. Electromagnetic phased array theory should be studied to determine if some of the work done in this area can be applied to ultrasonic phased arrays.

APPENDIX

COMPUTER PROGRAM LISTINGS

```
$BATCH
C   THIS PROGRAM PLOTS THE FAR FIELD PATTERN FOR A LINEAR
C  ULTRASOUND PHASED ARRAY AND COMPUTES THE PHASE ANGLES NEEDED
C  TO DRIVE EACH OF THE ELEMENTS OF THE ARRAY.  THE INPUTS ARE
C  BEAM STEERING ANGLE, DEPTH OF FOCAL POINT, WIDTH AND HEIGHT
C  OF THE ELEMENTS, NUMBER OF ELEMENTS AND FREQUENCY.
C
      DIMENSION FDIST(50), PHASE(50)
      REAL H,NF,I
C
C   INPUT THE ARRAY DATA.
C
      WRITE (1,10)
  10  FORMAT(' ELEMENT WIDTH, HEIGHT, SPACING (mm), AND NUMBER ?')
      READ (1,20) W,H,S,N
  20  FORMAT (F6.1,/,F6.1,/,F6.1,/,I2)
      WRITE (1,30)
  30  FORMAT(' DEPTH OF FOCUS (mm), BEAM STEERING ANGLE, ',
     $' AND FREQUENCY (MHz) ?')
      READ (1,40) Z,BD,F
  40  FORMAT (F6.1,/,F6.1,/,F10.4)
      WRITE (1,41)
  41  FORMAT (' PRINT ARRAY DATA ON SCREEN [1], OR PRINTER [3] ?')
      READ (1,415) NP
  415 FORMAT (I1)
      WRITE (1,42)
  42  FORMAT (' PLOT X-Z [0], OR Y-Z [1] PLANE ?')
      READ (1,43) L
  43  FORMAT (I1)
      IF (L.EQ.1) GO TO 47
      WRITE (1,44)
  44  FORMAT (' LENGTH OF + Xz AXIS TO BE PLOTTED (mm) ?')
      READ (1,46) FIN
  46  FORMAT (F6.1)
      GO TO 495
  47  WRITE (1,48)
  48  FORMAT (' LENGTH OF + Yz AXIS TO BE PLOTTED (mm) ?')
      READ (1,49) FIN
  49  FORMAT (F6.1)
C
C   CONVERT THE PHASE ANGLE FROM DEGREES TO RADIANS.
C
  495 B=BD/57.296
C
C   DETERMINE THE OVERALL WIDTH OF THE ARRAY.
C
      D=S*(N-1)+W
C
C   DETERMINE THE WAVELENGTH OF THE ULTRASOUND IN TISSUE.
C
      WL=1.5/F
C
C   DETERMINE WHETHER THE FOCUS IS IN THE NEAR OR FAR FIELD.
C
      NF=D**2/4./WL
      IF(Z.LT.NF) GO TO 50
```

```
      CALL FARFLD (W,WL,Z,B,D,H,S,N,F,FIN,L)
      GO TO 55
   50 WRITE (1,52)
   52 FORMAT (' FOCUS IN THE NEAR FIELD')
C
C   DETERMINE THE PHASE ANGLES NEEDED FOR EACH ELEMENT TO ACHIEVE
C  THE DESIRED FOCAL POINT.
C
   55 DO 60 J=1,N
      FDIST(J)=SQRT(Z**2+(D/2.+Z*TAN(B)-W/2.-(J-1)*S)**2)
   60 CONTINUE
      IF (B.LT.0.) GO TO 70
      RMAX=FDIST(1)
      GO TO 80
   70 RMAX=FDIST(N)
      PHAMAX=0.0
   80 DO 95 K=1,N
      PHASE(K)=((RMAX-FDIST(K))/WL)*360./WL
   90 IF (PHASE(K).LT.360.) GO TO 92
      PHASE(K)=PHASE(K)-360.
      GO TO 90
   92 IF (PHAMAX.GT.PHASE(K)) GO TO 93
      PHAMAX=PHASE(K)
   93 PHASE(K)=-PHASE(K)
   95 CONTINUE
      DO 100 K=1,N
      PHASE(K)=PHASE(K)+PHAMAX
  100 CONTINUE
C
C   PRINT ARRAY DIMENSIONS AND ELEMENT PHASE SHIFTS.
C
      WRITE (NP,101)
  101 FORMAT ('1',23X,' ARRAY PARAMETERS',///)
      WRITE (NP,102) N,W,H
  102 FORMAT (20X,' NUMBER OF ELEMENTS = ',I2,//,20X,
     $' ELEMENT WIDTH = ',F6.1,'  mm',//,20X,' ELEMENT HEIGHT = ',
     $F6.1,'  mm',/)
      WRITE (NP,104) S,D,Z
  104 FORMAT (20X,' ON CENTER SPACING = ',F6.1,'  mm',//,20X,
     $' WIDTH OF ARRAY = ',F6.1,'  mm',//,20X,
     $' DEPTH OF FOCUS = ',F6.1,'  mm',/)
      WRITE (NP,106) BD,F
  106 FORMAT(20X,' BEAM STEERING ANGLE = ',F6.1,'  degrees',//,
     $20X,' FREQUENCY = ',F10.4,'  MHz',////)
      WRITE (NP,108)
  108 FORMAT (17X,' PHASE SHIFTS REQUIRED FOR FOCUS',///)
      DO 120 M=1,N
      MN=M-1
      WRITE (NP,110) MN,PHASE(M)
  110 FORMAT (19X,' ELEMENT ',I2,' : ',F6.1,' degrees',/)
  120 CONTINUE
      WRITE (NP,125)
  125 FORMAT ('1')
      STOP
      END
C
```

```
C   THIS SUBROUTINE DETERMINES THE FAR FIELD PATTERN FOR
C  THE ARRAY AND CALLS A PLOTTING ROUTINE TO MAKE A TWO DIMENSIONAL
C  PLOT OF THE RESULT.
C
      SUBROUTINE FARFLD (W,WL,Z,B,D,H,S,N,F,FIN,L)
      DIMENSION XAX(103), ZAX(103), YAX(103), ZAY(103)
      ZAXMAX=0.
      DO 170 NX=1,101
      XZ=-FIN+(NX-1)*FIN/50.
      XAX(NX)=XZ
      T=(XZ*W/WL/SQRT(XZ**2+Z**2))*3.1416
      IF (T.NE.0.) GO TO 130
      SNC=1.
      GO TO 145
 130  SNC=(SIN(T))/T
 145  U=(N*S/WL)*(XZ/SQRT(XZ**2+Z**2)-SIN(B))*3.1416
      SINU=SIN(U/N)
      IF (SINU.NE.0.) GO TO 150
      ZAX(NX)=ZAX(NX-1)
      GO TO 170
 150  SNCD=SIN(U)/SINU
C
C   DETERMINE THE MAGNITUDE OF THE FIELD AMPLITUDE IN
C  THE X-Z PLANE.
C
      ZAX(NX)=ABS(SNC*SNCD*Z/SQRT(XZ**2+Z**2))
      IF (ZAXMAX.GT.ZAX(NX)) GO TO 170
      ZAXMAX=ZAX(NX)
 170  CONTINUE
C
C   NORMALIZE THE Z AXIS.
C
      DO 171 NX=1,101
      ZAX(NX)=10*ALOG10(ZAX(NX)/ZAXMAX)
 171  CONTINUE
      IF (L.NE.0) GO TO 172
C
C   PLOT THE FAR-FIELD PATTERN IN THE X-Z PLANE.
C
      CALL SPLOT (XAX,ZAX,B,W,Z,D,H,S,N,F,FIN,0)
      GO TO 192
 172  ZAYMAX=0.0
      DO 190 NY=1,101
      Y=-FIN+(NY-1)*FIN/50.
      YAX(NY)=Y
      YT=(Y*H/WL/Z)*3.1416
      IF (YT.NE.0.) GO TO 175
      SNCY=1.
      GO TO 180
 175  SNCY=(SIN(YT))/YT
C
C   DETERMINE THE MAGNITUDE OF THE FIELD AMPLITUDE IN
C  THE Y-Z PLANE.
C
 180  ZAY(NY)=ABS(ZAXMAX*SNCY)
      IF (ZAYMAX.GT.ZAY(NY)) GO TO 190
```

```
      ZAYMAX=ZAY(NY)
 190  CONTINUE
      DO 191 NY=1,101
      ZAY(NY)=10*ALOG10(ZAY(NY)/ZAYMAX)
 191  CONTINUE
C
C   PLOT THE FAR-FIELD PATTERN IN THE Y-Z PLANE.
C
      CALL SPLOT (YAX,ZAY,B,W,Z,D,H,S,N,F,FIN,1)
 192  RETURN
      END
C
C   THIS SUBROUTINE PLOTS A TWO DIMENSIONAL GRAPH OF DATA
C  PASSED TO IT IN TWO ARRAYS.
C
      SUBROUTINE SPLOT(XAXIS,YAXIS,B,W,Z,D,H,S,N,F,FIN,L)
      DIMENSION XAXIS(103),YAXIS(103)
      BD=B*57.296
      BZ=B*Z
      RN=N
      CALL PLOTS (0.01,8)
      CALL SYMBOL (1.5,12.,0.25,
     $'FAR-FIELD PATTERN OF A LINEAR ARRAY',0.,35)
C
C   PRINT LABELS DEPENDING ON WHICH PLANE IS TO BE PLOTTED.
C
      IF (L.EQ.0) GO TO 195
      CALL SYMBOL (3.5,11.5,.25,'(Xz =      mm)',0.,14)
      CALL NUMBER (4.75,11.5,.25,BZ,0.,1)
      GO TO 200
 195  CALL SYMBOL (4.,11.5,.25,'(Yz = 0.0 mm)',0.,13)
 200  CALL SYMBOL (1.0,1.4,.15,'NUMBER OF ELEMENTS = ',0.,21)
      CALL NUMBER (3.75,1.4,.15,RN,0.,-1)
      CALL SYMBOL (1.0,1.0,.15,'ELEMENT WIDTH      =       mm',
     $0.,29)
      CALL NUMBER (3.75,1.0,.15,W,0.,1)
      CALL SYMBOL (1.0,0.6,.15,'ELEMENT SPACING    =       mm',
     $0.,29)
      CALL NUMBER (3.75,0.6,.15,S,0.,1)
      CALL SYMBOL (1.0,0.2,.15,'ARRAY WIDTH        =       mm',
     $0.,29)
      CALL NUMBER (3.75,0.2,.15,D,0.,1)
      CALL SYMBOL (6.0,1.4,.15,'ELEMENT HEIGHT =       mm',0.,25)
      CALL NUMBER (8.25,1.4,.15,H,0.,1)
      CALL SYMBOL (6.0,1.0,.15,'DEPTH OF FOCUS =       mm',0.,25)
      CALL NUMBER (8.25,1.0,.15,Z,0.,1)
      CALL SYMBOL (6.,.6,.15,'BEAM STEERING  =      degrees',0.,29)
      CALL NUMBER (8.25,.6,.15,BD,0.,1)
      CALL SYMBOL (6.0,0.2,.15,'FREQUENCY      =         MHz',0.,28)
      CALL NUMBER (8.25,0.2,.15,F,0.,3)
C
C   PLOT THE YAXIS.
C
      CALL SCALE (YAXIS,8.0,101,1)
      FS=YAXIS(102)
      DS=YAXIS(103)
```

```
      CALL AXIS(1.,3.,'FIELD AMPLITUDE RELATIVE TO MAIN BEAM (db)',
     $0,8.,90.,FS,DS)
C
C    PLOT THE XAXIS.
C
      CALL SCALE (XAXIS,8.0,101,1)
      XAXIS(102)=-FIN
      XAXIS(103)=FIN/4.
      IF (L.EQ.0) GO TO 205
      CALL AXIS (1.,3.,' ',-1,8.,0.,-FIN,XAXIS(103))
      GO TO 210
 205  CALL AXIS (1.,3.,' ',-1,8.,0.,-FIN,XAXIS(103))
 210  CALL PLOT (1.,3.,-3)
C
C    PLOT THE FIELD PATTERN.
C
      CALL LINE (XAXIS,YAXIS,101,1,0,0)
      CALL PLOT (0.,0.,10)
      CALL PLOT (0.,0.,11)
      RETURN
      END
$BEND
```

```
C   THIS PROGRAM LOADS THE COUNTERS OF EACH ELEMENT OF THE ARRAY
C  WITH THE DESIRED ATTENUATION AND PHASE SHIFT.  THE INPUTS ARE
C  ELEMENT NUMBER, ATTENUATION, AND PHASE ANGLE.
C
      INTEGER*4 R(4),T1,T2
      PI=3.1416
1     CONTINUE
C
C   ENTER THE ELEMENT NUMBER, PHASE, AND ITS ATTENUATION FROM
C  ITS MAXIMUM AMPLITUDE.
C
      WRITE(1,5)
5     FORMAT('ENTER ELEMENT NUMBER, ATTENUATION, AND PHASE')
      READ(1,10)NUM
10    FORMAT(I1)
      IF(NUM.GE.7) GOTO 25
      READ(1,15)AMP,PHI
15    FORMAT(F16.8)
      AMP=10.0**(-AMP/20.0)
      AMP=128.0/PI*ATAN(SQRT(1-AMP**2)/AMP)
      PHI=128.0*PHI/180.0
C
C   CALCULATE THE VALUES TO PROGRAM THE TWO SETS OF COUNTERS
C  BASED ON THE ATTENUATION AND PHASE.
C
      T1=IFIX((PHI+AMP)/2.0)
      T2=IFIX((PHI-AMP)/2.0)
C
C   LOAD COUNTERS
C
$ASSM
         STM   12,R
         LHI   15,X'00A8'
         LHI   14,X'6A00'
         WHR   15,14
         BAL   13,WATE
         L     14,NUM
         OHI   14,X'6B00'
         WHR   15,14
         BAL   13,WATE
         L     14,T1
         NHI   14,X'007F'
         OHI   14,X'6C00'
         WHR   15,14
         BAL   13,WATE
         L     14,T2
         NHI   14,X'007F'
         OHI   14,X'6D00'
         WHR   15,14
         B     EXIT
WATE     LHI   12,40
LOOP     SIS   12,1
         BNZS  LOOP
         BR    13
EXIT     LM    12,R
$FORT
```

```
C
C    CALCULATE THE ACTUAL PHASE AND ATTENUATION THAT THE COUNTERS
C   WILL PRODUCE.
C
      AMP=-20.0*ALOG10(COS(PI*FLOAT(T1-T2)/128.0))
      PHI=180.0*FLOAT(T1+T2)/128.0
      WRITE(1,20)AMP,PHI
 20   FORMAT(' ATTENUATION = ',F7.3,' DB',8X,' PHASE = ',F7.3,
     $' DEGREES',/)
      GOTO 1
 25   WRITE(1,30)
 30   FORMAT('START COUNTERS ?  YES [1] OR NO [0]')
      READ(1,35)IAN
 35   FORMAT(I1)
      IF(IAN.NE.1) GOTO 40
C
C    START COUNTERS
C
$ASSM
         STM    14,R
         LHI    15,X'00A8'
         LHI    14,X'6A01'
         WHR    15,14
         LM     14,R
$FORT
      GOTO 1
 40   STOP
      END
```

REFERENCES

Aero-Tech Report (1981). "Linear Arrays: Theory of Operation and Performance," Kautkramer-Branson, INC., 2(1), 1-8.

Christensen, D. A. and Durney, C. H., (1981). "Hyperthermia Production for Cancer Therapy A Review of Fundamentals and Methods," J. Microwave Power, 16(2), 89-105.

Dias, J. F., (1982). "An Experimental Investigation of the Cross-Coupling Between Elements of an Acoustic Imaging Array Transducer," Ultrasonic Imaging, 4, 44-55.

Hynynen, K., Watmough, D. J., and Mallard, J. R., (1981). "Design of Ultrasonic Transducers for Local Hypethermia," Ultrasound Med. Biol., 7(4), 397-402.

Larson, J., (1981). "Non-ideal Radiators in Phased Array Transducers," 1981 Ultrasonics Symposium Proceedings, 673-684.

Lele, P. P., (1975). "Hyperthermia by Ultrasound," Proc. of the International Symposium on Cancer Therapy by Hyperthermia and Radiation, 168-178.

Macovski, A., (1979). "Ultrasonic Imaging Using Arrays," Proceedings of the IEEE, 67(4), 484-495.

Selfridge, A. R., Kino, G. S., and Khuri-Yakub, B. T., (1980). "A Theory for the Radiation Pattern of a Narrow Strip Acoustic Transducer," Appl. Phys. Lett., 37(1), 35-36.

Vaughn, S. T., (1980). "Automation of Ultrasound Dosimetry Experiment," Masters Thesis, University of Illinois.